

# Neuronal Store-Operated Calcium Entry Pathway as a Novel Therapeutic Target for Huntington's Disease Treatment

Jun Wu,<sup>1,4</sup> Hsin-Pei Shih,<sup>2,4,5</sup> Vladimir Vigont,<sup>3,4</sup> Lori Hrdlicka,<sup>2</sup> Len Diggins,<sup>2</sup> Carol Singh,<sup>2</sup> Matt Mahoney,<sup>2</sup> Richard Chesworth,<sup>2</sup> Gideon Shapiro,<sup>2</sup> Olga Zimina,<sup>3</sup> Xuesong Chen,<sup>1</sup> Qingqing Wu,<sup>1</sup> Lyubov Glushankova,<sup>3</sup> Michael Ahljanian,<sup>2,6</sup> Gerhard Koenig,<sup>2</sup> Galina N. Mozhayeva,<sup>3</sup> Elena Kaznachejeva,<sup>3</sup> and Ilya Bezprozvanny<sup>1,\*</sup>

<sup>1</sup>Department of Physiology, UT Southwestern Medical Center, Dallas, TX 75390, USA

<sup>2</sup>EnVivo Pharmaceuticals, Watertown, MA 02472, USA

<sup>3</sup>Institute of Cytology, Russian Academy of Sciences, St. Petersburg 194064, Russia

<sup>4</sup>These authors contributed equally to this work

<sup>5</sup>Present address: Vertex Pharmaceuticals Inc, 130 Waverly Street, Cambridge, MA 02139, USA

<sup>6</sup>Present address: Bristol Myers Squibb, 5 Research Parkway, Wallingford, CT 06492, USA

\*Correspondence: Ilya.Bezprozvanny@UTSouthwestern.edu

DOI 10.1016/j.chembiol.2011.04.012

## SUMMARY

Huntington's disease (HD) is a neurodegenerative disorder caused by a polyglutamine expansion within Huntingtin (Htt) protein. In the phenotypic screen we identified a class of quinazoline-derived compounds that delayed a progression of a motor phenotype in transgenic *Drosophila* HD flies. We found that the store-operated calcium (Ca<sup>2+</sup>) entry (SOC) pathway activity is enhanced in neuronal cells expressing mutant Htt and that the identified compounds inhibit SOC pathway in HD neurons. The same compounds exerted neuroprotective effects in glutamate-toxicity assays with YAC128 medium spiny neurons primary cultures. We demonstrated a key role of TRPC1 channels in supporting SOC pathway in HD neurons. We concluded that the TRPC1-mediated neuronal SOC pathway constitutes a novel target for HD treatment and that the identified compounds represent a novel class of therapeutic agents for treatment of HD and possibly other neurodegenerative disorders.

## INTRODUCTION

Huntington's disease (HD) is an inherited autosomal dominant neurodegenerative disorder caused by a polyQ expansion (>36 glutamine repeats) in Huntingtin (Htt) protein (Huntington's Disease Collaborative Research Group, 1993). The pathological hallmark of HD is the loss of medium spiny neurons (MSN) in the striatum, which accounts for the major clinical symptoms of the disease. The clinical picture of HD include chorea, psychiatric disturbance, gradual dementia, and death (Vonsattel and DiFiglia, 1998). The exact cause of striatal neuronal loss in HD remains elusive. Diverse pathological paradigms of HD have been proposed such as transcriptional dysregulation, oxidative stress, mitochondrial dysfunction, ubiquitin-proteasome system

impairment, and aberrant caspase activation (Cha, 2007; Gil and Rego, 2008; Imarisio et al., 2008; Petrucelli and Dawson, 2004; Roze et al., 2008; Zhang et al., 2006). Growing evidence has suggested that abnormalities in Ca<sup>2+</sup> signaling play an important role in pathogenesis of HD (Bezprozvanny, 2009; Tang et al., 2005). Dopamine signaling antagonist tetrabenazine (selective VMAT2 inhibitor) has been recently approved by the Food and Drug Administration for treatment of HD symptoms in the United States (Bezprozvanny, 2009; Huntington Study Group, 2006). There is no disease-modifying therapy currently available to prevent the onset of HD symptoms or slow the progression of the disease.

The usual approach to drug discovery is based on developing drugs against previously validated targets, but the target-based approach has not been successful in developing HD therapeutics so far. Another approach is based on phenotypic screens in animal models of the disease. The advantage of phenotypic screening strategy is that it facilitates discovery of potential hits without prior assumptions about pathogenic mechanisms and in the context of the biological complexity that in vitro and cell-based models cannot easily achieve (Marsh et al., 2009). To identify potential HD therapeutic agents, we established a phenotypic screen by taking an advantage of *Drosophila* transgenic HD model that has been previously described (Al-Ramahi et al., 2006). In our experiments a small molecule quinazoline-derived compound library was screened for compounds that were able to delay progression of a motor phenotype in transgenic flies after induction of human Htt-128Q fragment expression. As a result of the screen we identified a number of hits that alleviated phenotype of transgenic HD flies.

Evaluation of obtained hits revealed that the same compounds have been previously isolated as inhibitors of nuclear factor- $\kappa$ B (NF- $\kappa$ B) pathway activation in immune cells (Tobe et al., 2003b). It has been previously suggested that these compounds do not inhibit NF- $\kappa$ B directly but act by blocking store-operated calcium (Ca<sup>2+</sup>) entry (SOC) (Choi et al., 2006), a critical step upstream of NF- $\kappa$ B activation in immune cells. An importance of SOC pathway for neuronal physiology was highlighted in recent studies of STIM2 knockout mice (Berna-Erro et al., 2009), genetic studies in *Drosophila* (Hasan and Venkiteswaran,

2010; Venkiteswaran and Hasan, 2009) and in recent functional studies with neuronal cultures (Gruszczynska-Biegala et al., 2011). In our studies we evaluated activity of isolated compounds as SOC inhibitors in HD neurons and validated their neuroprotective effects in experiments with MSN cultures from YAC128 transgenic mice. We discovered that the neuroprotective effects observed in *Drosophila* HD and YAC128 MSN assays were well correlated with ability of these compounds to inhibit activity of NF- $\kappa$ B and SOC pathways. We also discovered that neuronal SOC pathway is significantly upregulated in mutant Huntingtin expressing neurons. Based on these results we concluded that SOC pathway constitute a novel therapeutic target for treatment of HD and possibly other neurodegenerative disorders.

## RESULTS

### EVP4593 Is an NF- $\kappa$ B Pathway Inhibitor Isolated in the Phenotypic Screen with *Drosophila* HD Transgenic Model

Photoreceptor-specific expression of the exon 1-4 fragment of a human *huntingtin* gene with 128Q expansion in *Drosophila* has been reported to result in a neurodegenerative phenotype (Al-Ramahi et al., 2006). We discovered that expression of the same Htt-128Q transgene under control of pan-neuronal promoter leads to progressively impaired motor performance of transgenic HD flies with limb tremors and decreased climbing speed. The motor phenotype developed by transgenic HD flies can be quantified by dropping the flies to the bottom of the tube and measuring the speed of upward climbing for individual flies. On average the speed of upward climbing was reduced from 12 mm/s immediately after transgene expression to 5 mm/s 10 days after eclosion (Figure 1A, blue line). The climbing speed of control flies expressing LacZ transgene remained constant at 13 mm/s in the same time period (Figure 1A, red line). To validate this experimental system, we reconfirmed efficacy of several pharmacological compounds published in the previous studies with *Drosophila* HD models, such as histone deacetylase inhibitor inhibitors TSA (Figure 1A, green line) and SAHA (data not shown) and rapamycin (data not shown) (Ravikumar et al., 2004; Steffan et al., 2001). Thus, we concluded that the reproducible, progressive and quantifiable motor deficit observed in transgenic HD flies (Figure 1A) provides an opportunity for screening for novel potential HD therapeutic agents.

In search for such agents we screened a quinazoline-derived small molecule library composed of 521 compounds using the climbing assay as readout and identified several initial hits. The initial hits were used in a structure similarity search and a secondary focused library of additional 72 quinazoline-derived compounds was generated and screened. As a result of the secondary focused library screening we discovered EVP4593 as a potent hit. This compound significantly slowed the progressive decline in the climbing speed of the HD flies (Figure 1A, yellow line). The efficacy of EVP4593 at 400  $\mu$ M in the climbing assay was superior to the efficacy of TSA at 250  $\mu$ M (Figure 1A), which was used as a positive control in our experiments (Steffan et al., 2001). The efficacy of TSA at 400  $\mu$ M could not be tested because of toxicity observed at TSA concentrations above

250  $\mu$ M (data not shown). To quantify the effects of EVP4593, we measured an average improvement in the climbing speed when compared to HD transgenic flies feed with 1% dimethyl sulfoxide (DMSO). To calculate a magnitude of the observed effects, the difference in the average climbing speed of HD flies resulting from EVP4593 feeding was normalized to the standard deviation in the climbing speed of the entire DMSO-treated group. When the data collected during days 8–10 after transgene induction were averaged, we determined that feeding the flies with 400  $\mu$ M of EVP4593 resulted in an average effect size of 3.0 ( $p < 0.003$ ) (Figure 1B). The efficacy of EVP4593 was dose-dependent in the range between 100  $\mu$ M and 400  $\mu$ M in the fly food (Figure 1B). The EVP4593 had no significant effect on climbing performance of HD flies at 50  $\mu$ M (Figure 1B). The EVP4593 had no toxic effects on *Drosophila* in the range of concentrations tested in our assays (50–400  $\mu$ M).

EVP4593 is a derivative of 6-aminoquinazoline class (Figure 1C) that has been previously isolated as an inhibitor of PMA/PHA-induced NF- $\kappa$ B pathway activation in Jurkat cells (Tobe et al., 2003b). To determine if the beneficial effects observed in the climbing assay with transgenic HD flies (Figure 1A) are related to inhibition of NF- $\kappa$ B signaling, we selected seven structural analogs of EVP4593 from the same chemical class (Figure 1C). The efficacy of each of these compounds was evaluated in the climbing assay with HD flies and in PMA/PHA-induced NF- $\kappa$ B assay with human Jurkat cells. The effect size in the climbing assay was measured in the presence of 200  $\mu$ M of each tested compound in the fly food at days 8–10 after Htt-128Q transgene induction. The inhibition of NF- $\kappa$ B activation was evaluated at 1  $\mu$ M of each compound. We found that EVP4593, EVP14782, and EVP14756 demonstrated significant potency in climbing assay with effect sizes in the range of 2–4 ( $p < 0.003$ ) (Figure 1D). In contrast, EVP14809, EVP14810, EVP14812, and EVP14808 compounds were inactive in the climbing assay (Figure 1D). When evaluated in NF- $\kappa$ B assay, compounds EVP4593, EVP14782, and EVP14756 were also most potent with 50%–60% inhibition (Figure 1D). Compounds EVP14809 and EVP14810 were less potent with 20% inhibition and compounds EVP14812, and EVP14808 were unable to inhibit NF- $\kappa$ B activation (Figure 1D).

To get more insight into mechanism of action of these compounds, we evaluated dose-dependence of NF- $\kappa$ B pathway inhibition by these compounds. We discovered that EVP4593, EVP14782, and EVP14756 acted as high affinity partial antagonists of NF- $\kappa$ B pathway activation. These three compounds inhibited 50%–60% of NF- $\kappa$ B activity with apparent affinities in the nanomolar range (see Figure S1 available online; Table 1). Compounds EVP14809 and EVP14810 also acted as partial antagonists of NF- $\kappa$ B activation but with affinities in the micromolar range (Figure S1; Table 1). The compounds EVP14812 and EVP14808 were not able to inhibit NF- $\kappa$ B activation (Figure S1; Table 1). Our analysis revealed excellent correlation between ability of compounds in this chemical series to inhibit PMA/PHA-induced NF- $\kappa$ B activation in human Jurkat cells and to alleviate motor symptoms developed by transgenic HD flies (Figure 1D and Table 1). This correlation was further confirmed by testing 30 more additional analogs from the same chemical class with various potencies of NF- $\kappa$ B inhibition (data not shown).

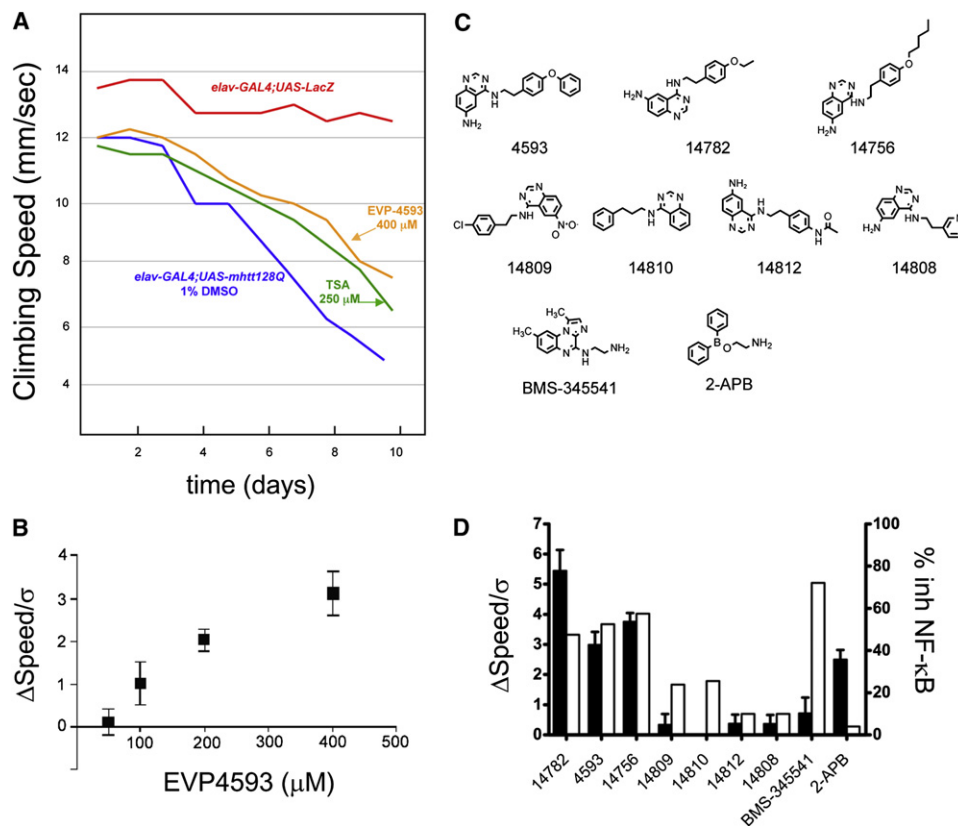


**Figure 1. Identification of EVP4593 in Climbing Assay Screen with Huntington's Disease Transgenic Flies**

(A) The climbing speed of HD flies is plotted as a function of time after induction of mHtt-128Q transgene. The results with lacZ-expressing flies are shown as a control (red). A number of small molecule compounds were dissolved in dimethyl sulfoxide (DMSO) and included in the fly food in the final concentration as indicated. The results obtained in HD flies for 400  $\mu$ M EVP4593 (orange), 250  $\mu$ M TSA (green) and 1% DMSO (blue) are compared.

(B) Dose-dependence of EVP4593 in rescuing motor dysfunction of HD flies. An average effect size relative to 1% DMSO control was determined at days 8–10 after mHtt-128Q transgene induction ( $\Delta$ Speed), normalized to variability of the climbing speed in DMSO-treated group ( $\sigma$ ) and plotted as mean  $\pm$  SE (n = 30 flies) against concentration of EVP4593 in the fly food.

(C) Chemical structures of EVP4593 and its analogs used in the study. BMS-345541 is an unrelated compound with potent IKK inhibitory activity. 2-APB is an unrelated compound with ability to block SOC with low affinity in some cell types.

(D) The potency of 200  $\mu$ M of EVP4593 or its analogs in the climbing assay was determined as an average effect size at days 8–10 after mHtt-128Q transgene induction and shown as mean  $\pm$  SE (n = 30 flies) (filled bars). The potency of 1  $\mu$ M of EVP4593 or its analogs was determined as percent inhibition of NF- $\kappa$ B activity and shown as mean  $\pm$  SE (n = 4–6) (open bars). Also shown are results for BMS-345541 and 2-APB (400  $\mu$ M in climbing assay and 1  $\mu$ M in NF- $\kappa$ B assay for both compounds).

See also Figure S1.

To determine if direct inhibition of NF- $\kappa$ B is responsible for beneficial effects observed in the climbing assay, we evaluated structurally unrelated compound BMS-345541 (Figure 1C). BMS-345541 is a potent I $\kappa$ B kinase (IKK) inhibitor (Burke et al., 2003), which fully and with high affinity suppressed PMA/PHA-induced NF- $\kappa$ B activation in Jurkat cells in our experiments (Figure 1D; Figure S1). However, BMS-345541 at 400  $\mu$ M was inactive when tested in the climbing assay with transgenic HD flies (Figure 1D). Similarly negative results were obtained in experiments with several additional IKK inhibitors tested in the climbing assay with transgenic HD flies (data not shown). In contrast, EVP4593 was not active when tested in the IKK kinase assay (data not shown). These data suggested that direct inhibition of NF- $\kappa$ B may not be responsible for the beneficial effects observed with EVP4593, EVP14782, and EVP14756 compounds in the climbing assays.

The library of quinazoline class of compounds was chosen initially for our screen as this scaffold often leads to kinase inhibitors, and kinases are considered attractive and tractable drug targets. However, when EVP4593 compound was evaluated at 10  $\mu$ M concentration in commercial kinase inhibition assays using screening platforms from MDS Pharma Services, Ambit Biosciences, and Millipore we could not detect significant kinase inhibitory activity for this compound (data not shown). All these results suggested that EVP4593 and its active analogs EVP14782 and EVP14756 are likely to inhibit NF- $\kappa$ B activation indirectly. This conclusion is consistent with the partial antagonism displayed by these compounds when tested in PMA/PHA-induced NF- $\kappa$ B activation assay (Figure S1), in contrast to the full antagonism displayed in the same assay by BMS-345541 (Figure S1). PMA/PHA-induced NF- $\kappa$ B activation depends on activation of protein kinase C (PKC) and Ca<sup>2+</sup> influx.

**Table 1. Performance of EVP4593 and Its Analogs in Different Assays**

EVP Compound	HD Flies Climbing Assay (200 $\mu$ M)	NF- $\kappa$ B Inhibition (EC <sub>50</sub> , nM)	SOC Inhibition (Ca <sup>2+</sup> assay, 0.3 $\mu$ M)	SOC Inhibition (Mn <sup>2+</sup> assay, 0.3 $\mu$ M)	SOC Inhibition (Ephys assay, 0.3 $\mu$ M)	In Vitro HD Assay (0.03–3.0 $\mu$ M)
14782	+	7	ND	+	ND	+
4593	+	9	+	+	+	+
14756	+	66	+	+	ND	+
14809	–	1150	ND	ND	ND	+/–
14810	–	1203	ND	–	ND	–
14812	–	8934	ND	–	ND	–
14808	–	>10,000	–	–	–	–

Ephys, electrophysiological; HD, Huntington's disease; ND, not determined; SOC, store-operated calcium current.

We determined that EVP4593 does not inhibit PKC in vitro kinase assays (data not shown). Thus, we hypothesized that EVP4593 may act by inhibiting store-operated Ca<sup>2+</sup> entry (SOC), a critical upstream step of NF- $\kappa$ B activation in Jurkat cells. Indeed, it has been previously reported that EVP4593 can inhibit SOC in experiments with SH-5Y5 cells (Choi et al., 2006). To test this possibility, we evaluated structurally distinct 2-APB compound (Figure 1C) that is known to act as low affinity SOC inhibitor in some cells (Bootman et al., 2002; Ma et al., 2003). We discovered that when added to fly food at 400  $\mu$ M, 2-APB also demonstrated significant benefit in the climbing assay (Figure 1D). Interestingly, at 1  $\mu$ M concentration 2-APB did not inhibit NF- $\kappa$ B activation (Figure 1D), indicating that SOC pathway in Jurkat cells is not efficiently blocked by 2-APB. Based on these results we proposed that EVP4593 and its active analogs EVP14782 and EVP14756 might exert beneficial effect by inhibiting SOC Ca<sup>2+</sup> entry pathway in neurons of HD flies. To test this hypothesis we set out to determine if EVP4593 and its active analogs act by inhibiting SOC pathway in neuronal cells.

#### EVP4593 and Its Active Analogs Inhibit Store-Operated Ca<sup>2+</sup> Entry in HD Striatal Neurons

In our studies, we focused on medium spiny striatal neurons (MSN), the main locus of pathology in HD. In the first series of experiments we evaluated the size of SOC in wild-type (WT) MSN and YAC128 MSN. The WT and YAC128 MSN were incubated in Ca<sup>2+</sup>-free media in the presence of 1  $\mu$ M of SERCA pump inhibitor thapsigargin (Tg) for 5 min to cause complete depletion of intracellular Ca<sup>2+</sup> stores. After complete store depletion the neurons were transferred to the extracellular media containing 2 mM Ca<sup>2+</sup> and the amplitude of initial cytosolic Ca<sup>2+</sup> influx after Ca<sup>2+</sup>-re-addition was determined by Fura-2 imaging. In these experiments we observed that the amplitude of SOC Ca<sup>2+</sup> entry was significantly higher in YAC128 MSN (Figure 2B) than in WT MSN (Figure 2A). On average, the amplitude of SOC Ca<sup>2+</sup> entry was 0.21  $\pm$  0.02 (n = 38) in WT MSN and 0.30  $\pm$  0.02 (n = 29) in YAC128 MSN (p < 0.05) (Figure 2E). We also found the thapsigargin-induced Ca<sup>2+</sup> release from the ER was reduced in YAC128 MSN when compared with WT (Figures 2A and 2B). Most likely this is due to increased sensitivity of InsP<sub>3</sub>R1 to activation by InsP<sub>3</sub> caused by the presence of the mutant Htt (Tang et al., 2003), which causes increased ER Ca<sup>2+</sup> leakage at the steady-state conditions. Addition of

300 nM of EVP4593 resulted in strong attenuation of SOC Ca<sup>2+</sup> influx in YAC128 MSN neurons (Figure 2D). On average the amplitude of SOC Ca<sup>2+</sup> entry in YAC128 MSN was reduced from 0.30  $\pm$  0.02 (n = 29) in the presence of DMSO control to 0.11  $\pm$  0.02 (n = 54) in the presence of 300 nM of EVP4593 (p < 0.001) (Figure 2E). Similar suppression of SOC Ca<sup>2+</sup> entry was also observed in the presence of 300 nM EVP14756 (Figure 2E). In contrast, inactive analog EVP14808 had no effect on the amplitude of SOC Ca<sup>2+</sup> entry in YAC128 MSN cells when tested in the same concentration (Figure 2E). Interestingly, SOC pathway in WT neurons was much less sensitive to inhibition by EVP4593. Addition of 300 nM EVP4593 did not inhibit Ca<sup>2+</sup> increase in WT neurons (Figure 2C) and had no significant effect on the amplitude of SOC-mediated Ca<sup>2+</sup> elevation in WT neurons (Figure 2E).

To quantitatively compare ability of EVP4593 and its analogs to inhibit SOC pathway in YAC128 MSN, we performed a series of measurements using Mn<sup>2+</sup>-induced Fura-2 quenching method (Dadsetan et al., 2008; Yang et al., 2005). In our experiments YAC128 MSN were loaded with Fura-2 and incubated in Ca<sup>2+</sup>-free media in the presence of 30  $\mu$ M of SERCA pump inhibitor CPA for 10 min to completely deplete Ca<sup>2+</sup> stores and to activate SOC pathway. After addition of 150  $\mu$ M Mn<sup>2+</sup> to the extracellular solution, Fura-2 quenching was initiated and initial slope of the F<sub>360</sub> decline was measured (Figure 3A, section a). Five minutes later 1‰ DMSO control or test compounds in 300 nM concentration were added and the rate of Fura-2 quenching was measured again (Figure 3A, section b). The effect of test compounds on SOC activity was estimated by comparing the slope of Fura-2 Mn<sup>2+</sup> quenching before (Figure 3A, section a) and after (Figure 3A, section b) addition of the compounds for each cell. In these experiments we found that an addition of DMSO had no effect on the rate of Fura-2 Mn<sup>2+</sup> quenching (Figure 3A). In contrast, addition of EVP4593 resulted in significant reduction in the rate of Fura-2 Mn<sup>2+</sup> quenching (Figure 3B). The inactive analog EVP14808 had no significant effect on the Fura-2 Mn<sup>2+</sup> quenching rate (Figure 3C). To compare results obtained in different experiments, we calculated the ratio of the Fura-2 Mn<sup>2+</sup> quenching rates observed after (phase b) and before (phase a) addition of the test compounds to each cell. From this analysis we determined that EVP4593, EVP14756 and EVP14782 compounds inhibited SOC pathway activity by ~40% when tested at 300 nM (Figure 3D and Table 1). In contrast, inactive

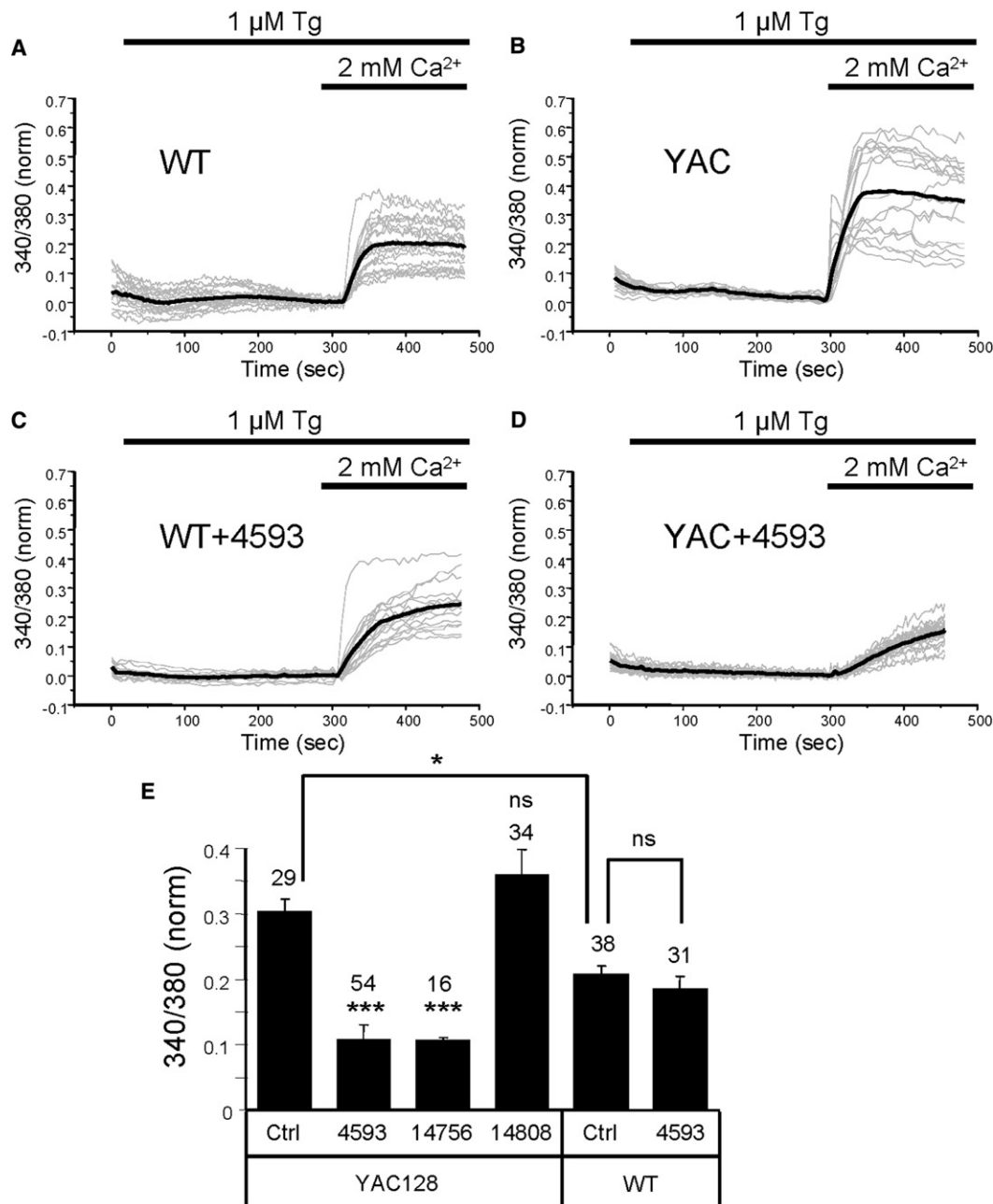


**Figure 2. Store-Operated Calcium Pathway in Wild-Type and YAC128 MSNs- $\text{Ca}^{2+}$  Imaging Assay**

(A and B) WT (A) and YAC128 (B) medium spiny neurons (MSN) cultures at DIV10–14 were loaded with Fura-2  $\text{Ca}^{2+}$  imaging dye and incubated in  $\text{Ca}^{2+}$ -free media. The intracellular  $\text{Ca}^{2+}$  stores were depleted by addition of  $1\ \mu\text{M}$  of thapsigargin (Tg) as indicated. Re-addition of  $2\ \text{mM}\ \text{Ca}^{2+}$  to the extracellular media resulted in  $\text{Ca}^{2+}$  influx via SOC pathway. Fura-2 340/380 ratio traces are shown for individual cells (gray thin lines). For each cell 340/380 ratio trace was offset to 0.0 for the time point of  $\text{Ca}^{2+}$  re-addition. The average trace is also shown (black thick line).

(C and D) SOC  $\text{Ca}^{2+}$  imaging experiments were performed with WT (C) and YAC128 (D) MSN in the presence of  $300\ \text{nM}$  EVP4593.

(E) An average amplitude of an increase in 340/380 Fura-2 signals in response to  $\text{Ca}^{2+}$  re-addition is shown for YAC128 and WT MSN in the presence of DMSO or  $300\ \text{nM}$  of test compounds as indicated. The results are shown as mean  $\pm$  SE (number of cells is shown on the top of the bar). \* $p < 0.05$ ; \*\*\* $p < 0.001$  when compared to DMSO group. ns, nonsignificant.

analogs EVP14808 and EVP14810 had no significant effect on SOC activity (Figure 3D and Table 1) and EVP14812 appeared to increase the rate of Fura-2  $\text{Mn}^{2+}$  quenching (Figure 3D and

Table 1). The EVP14809 caused interference with the  $\text{Mn}^{2+}$  quenching assay and the potency of this compound could not be evaluated by this approach.

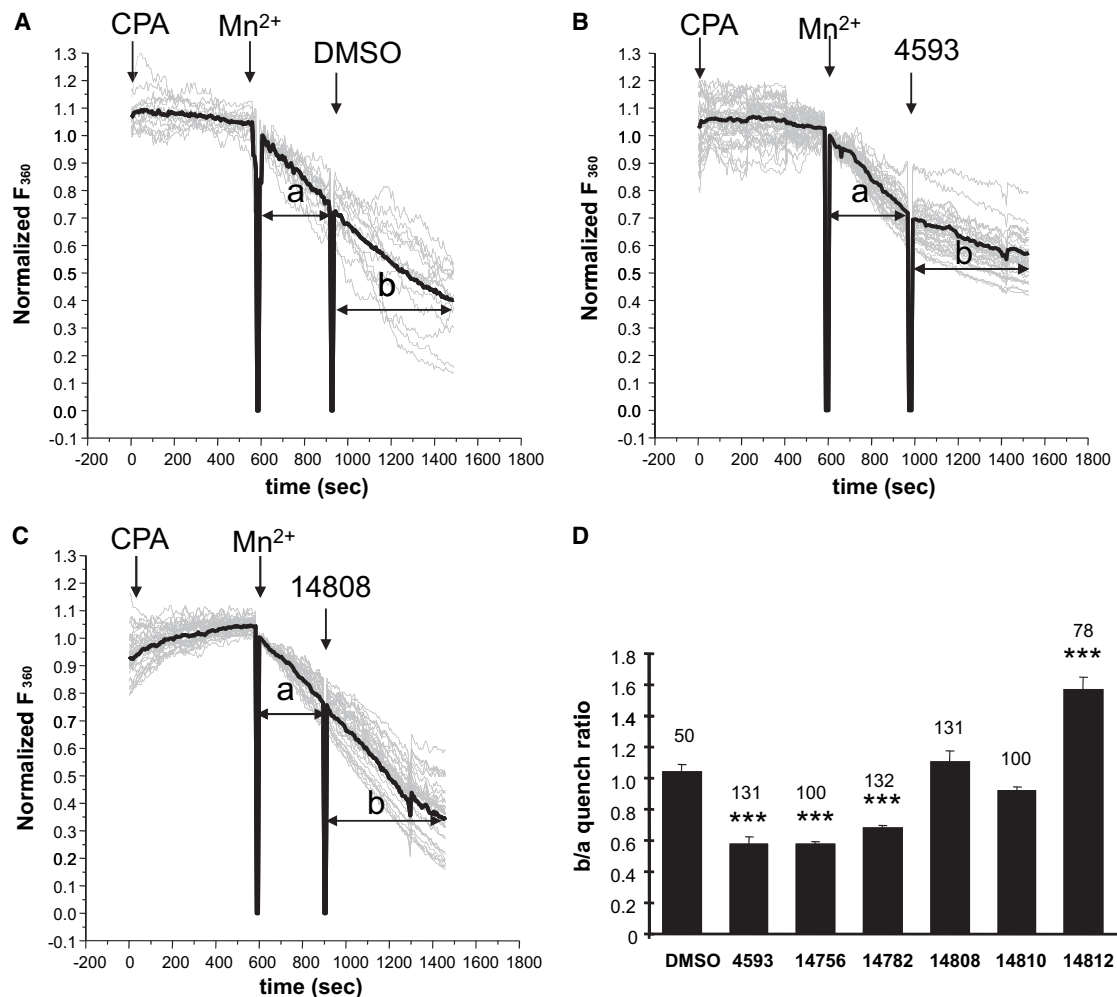


**Figure 3. SOC Pathway in YAC128 MSNs-Mn<sup>2+</sup> Quenching Assay**

(A–C) SOC pathway in YAC128 MSN is quantified by Mn<sup>2+</sup> quenching assay. The YAC128 MSNs loaded with Fura-2 were placed in Ca<sup>2+</sup>-free and Mn<sup>2+</sup>-free media containing 100 μM EGTA. The intracellular Ca<sup>2+</sup> stores are depleted by 10 min incubation with 30 μM of CPA. After addition of 150 μM of Mn<sup>2+</sup> to the extracellular media the Fura-2 quenching is quantified as reduction of the Fura-2 fluorescent signal at isobestic λ<sub>ex</sub> = 360 nm (F<sub>360</sub>). The rate of Fura-2 Mn<sup>2+</sup> quenching is calculated as the slope of the curve and determined for each cell before (phase a) and after (phase b) addition of DMSO (A), 300 nM of EVP4593 (B) or 300 nM EVP14808 (C). Fura-2 F<sub>360</sub> traces are shown for individual cells (gray thin lines). For each cell F<sub>360</sub> signal was normalized to F<sub>360</sub> signal at the time point of Mn<sup>2+</sup> addition. The average trace is also shown (black thick line).

(D) The changes in Fura-2 Mn<sup>2+</sup> quench rates in YAC128 MSNs are plotted as b/a slope ratios for each compound tested at 300 nM concentration. The average b/a ratios for each compound are shown as mean ± SE (number of cells is indicated above each bar). \*\*\*p < 0.001 when compared with DMSO group.

### EVP4593 Inhibits TRPC1-Supported SOC Ca<sup>2+</sup> Currents in Neuronal Cells

To further evaluate an ability of EVP4593 to act as SOC inhibitors we performed a series of electrophysiological experiments. In initial experiments we attempted whole cell recordings of SOC currents in primary mouse MSN cultures. We were able to record thapsigargin-activated Ba<sup>2+</sup> currents in mouse MSN cultures at the magnitude of 1.0 ± 0.2 (n = 10) pA/pF (data not shown). However, these experiments were technically difficult and it was challenging to obtain stable SOC recordings in MSN primary cultures. Thus, for electrophysiological analysis we selected SK-N-SH human neuroblastoma cells transiently transfected with human Htt-15Q or Htt-138Q expression constructs. The Htt expression constructs were cotransfected with EGFP

plasmid and transfected cells were identified by GFP fluorescence. In whole cell recordings of Isoc activity we used 10 mM Ba<sup>2+</sup> as a charge carrier as we previously described for A431 cells (Gusev et al., 2003). Under these conditions, passive store depletion after addition of 1 μM thapsigargin (Tg) induced inward cation currents that reached the maximum within 3 min after addition of Tg (Figure 4A). In these experiments we found that amplitude of Isoc inward currents in nontransfected cells and in the cells transfected with Htt-15Q cells was practically indistinguishable (Figure 4A). At -80 mV holding potential the amplitude of maximal Isoc currents in both groups of cells was equal to 0.45 pA/pF (Figures 4A–4C). In contrast, Tg-induced Isoc currents in Htt-138Q cells were much larger (Figure 4A), with maximal currents reaching 2.3 pA/pF at -80 mV (Figures

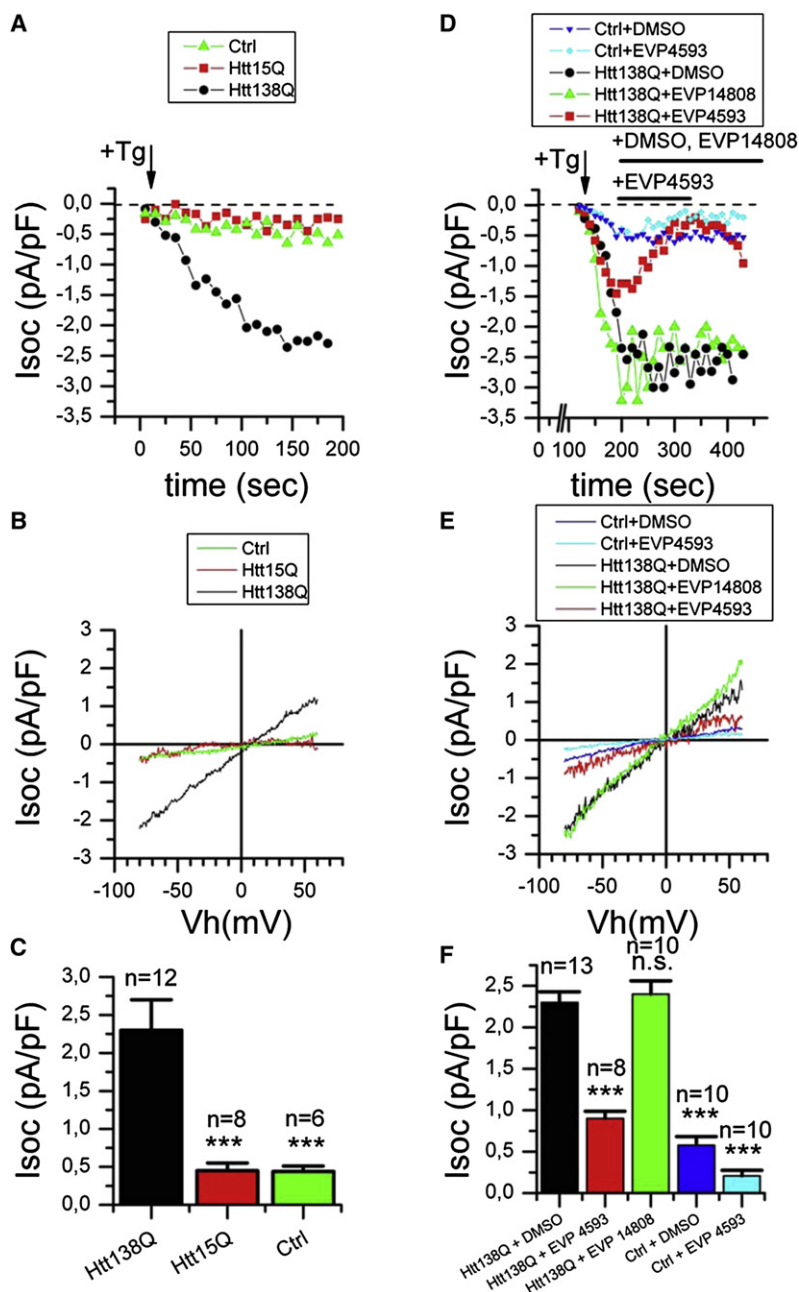


**Figure 4. Recordings of Isoc in SK-N-SH Cells Transfected with Htt-15Q and Htt-138Q**

(A) The amplitude of Isoc currents recorded in whole-cell experiments are shown as a function of time after application of 1  $\mu$ M Tg (indicated by arrow) to nontransfected SK-N-SH cells (Ctrl, green triangles) and to SK-N-SH cells transiently transfected with Htt-15Q (red squares) or Htt-138Q (black circles). The amplitude of Isoc currents for all groups of cells was measured every 10 s at  $-80$  mV test potential. Data from representative experiments are shown.

(B) The average current-voltage relationships recorded after full development of Isoc in nontransfected SK-N-SH cells (Ctrl, green trace) and SK-N-SH transiently transfected with Htt-15Q (red trace), or Htt-138Q (black trace). Each trace is an average based on a number of experiments as indicated in (C).

(C) The average Isoc amplitude in nontransfected SK-N-SH cells (Ctrl) and in SK-N-SH transfected with Htt-15Q or Htt-138Q constructs. For all groups of cells Isoc amplitude was determined at  $-80$  mV test potential and plotted as mean  $\pm$  SE ( $n$  = number of experiments). \*\*\* $p$  < 0.001 when compared to Htt138Q-transfected cells.

(D) Isoc currents in nontransfected SK-N-SH cells (Ctrl) and SK-N-SH cells transfected with Htt-138Q plasmid are shown as a function of the time after 1  $\mu$ M Tg application (indicated by arrow). The representative data obtained in the presence of DMSO (blue triangles for nontransfected cells and black circles for transfected cells), 300 nM EVP4593 (red squares for transfected cells and cyan rhombs for nontransfected cells), and 300 nM EVP14808 (green triangles for transfected cells) are shown. The amplitude of Isoc currents for all groups of cells was measured every 10 s at  $-80$  mV test potential. The times of EVP4593, EVP14808 and DMSO applications are shown above the Isoc plot.

(E) The average current-voltage relationships recorded after full development of Isoc in nontransfected SK-N-SH cells (Ctrl) and in SK-N-SH transfected with Htt-138Q in the presence of DMSO (blue trace for control cells and black trace for transfected cells), 300 nM EVP4593 (cyan trace for control cells and red trace for transfected cells), and 300 nM EVP14808 (green trace). Each trace is an average based on a number of experiments indicated in (F).

(F) The average Isoc amplitude in nontransfected (Ctrl) SK-N-SH cells and in SK-N-SH cells transfected with Htt-138 and recorded in the presence of DMSO, 300 nM EVP4593 or 300 nM EVP14808. For all groups of cells Isoc amplitude was determined at  $-80$  mV test potential and plotted as mean  $\pm$  SE ( $n$  = number of experiments). \*\*\* $p$  < 0.001 when compared to Htt138Q-transfected cells in the presence of DMSO.

4A–4C). On average, the amplitude of Isoc currents in SK-N-SH cells transfected with Htt-138Q plasmid was five times larger than in nontransfected cells or in the cells transfected with Htt-15Q plasmid (Figure 4C). The increased Isoc activity in electrophysiological experiments with neuronal cells transfected with Htt-138Q plasmid is consistent with increased SOC activity that we observed in  $Ca^{2+}$  imaging experiments with YAC128 MSNs (Figure 2).

To investigate the ability of EVP4593 to inhibit Isoc currents in SK-N-SH cells transfected with Htt-138Q, we applied 300 nM EVP4593 to the cells after Tg-induced Isoc current was fully activated. We found that addition of EVP4593 resulted in immediate

block of Isoc currents in these cells (Figure 4D). After washout of EVP4593 the amplitude of the Isoc current was partially recovered (Figure 4D), indicating that the inhibition was reversible. In contrast, addition of 300 nM EVP14808 had no effect on Isoc current in Htt-138Q transfected cells, similar to addition of DMSO carrier solution alone (Figure 4D). Addition of 300 nM EVP4593 resulted in  $\sim$ 2.5-fold reduction in the magnitude of Isoc currents recorded at  $-80$  mV holding potential in Htt-138Q-transfected cells (Figures 4D–4F). In contrast, addition of the same concentration of EVP14808 had no significant effect on Isoc currents in Htt-138Q-transfected cells (Figures 4D–4F). The small Isoc current in nontransfected SK-N-SH cells was

sensitive to EVP4593 (Figure 4D), but to a far lesser extent than Isoc current in Htt-138Q-transfected cells (Figures 4D–4F). This conclusion is consistent with results obtained in  $\text{Ca}^{2+}$  imaging experiments with WT and YAC128 MSN (Figure 2).

The molecular composition of neuronal SOC pathway is poorly understood, with potential components including members of mammalian Trp family and Orai1 channels (Berna-Erro et al., 2009; Gruszczynska-Biegala et al., 2011; Hasan and Venkiteswaran, 2010; Putney, 2003; Venkiteswaran and Hasan, 2009). Our electrophysiological measurements indicate that the channels upregulated in SK-N-SH cells in response to Htt-138Q transfection are relatively nonselective (Figure 4B), consistent with the known properties of mammalian TRPC channels (Montell, 2005). It has been recently demonstrated that together with Orai channels TRPC channels play an important role in supporting SOC in Jurkat cells (Wenning et al., 2011), and it is possible that EVP4593 inhibited TRPC-supported currents in our NF- $\kappa$ B activation experiments (Figure 1D). TRPC1 channels are expressed in the nervous system (Ricchio et al., 2002) and we reasoned that TRPC1 subunits may play a role in supporting Isoc currents upregulated in response to Htt-138Q expression. To test this hypothesis, we cotransfected SK-N-SH cells with Htt-138Q plasmid and siRNA plasmid against human TRPC1 subunit. Off-target control siRNA was used as a negative control in these experiments. Expression of endogenous TRPC1 in SK-N-SH cells and the efficiency of siRNA-mediated TRPC1 knockdown in transfected cells were confirmed by western blotting of cellular lysates (Figure S2). In these experiments we found that RNAi-mediated knockdown of TRPC1 significantly reduced Tg-induced Isoc currents in Htt-138Q-transfected cells (Figure 5A). At  $-80$  mV holding potential the amplitude of Isoc currents in these cells was equal to  $0.8$  pA/pF, comparable to the amplitude of Isoc currents in nontransfected cells (Figures 5A, 5C, and 5D). On average, cotransfection of Htt-138Q with TRPC1 RNAi plasmid reduced amplitude of Isoc currents by 70% (Figure 5D). The effect of TRPC1 RNAi was specific, as cotransfection of Htt-138Q with control RNAi had no effect on the amplitude of Isoc currents (Figures 5A, 5C, and 5D). In additional experiments we demonstrated that knockdown of TRPC1 by siRNA occluded effects of EVP4593 on Isoc currents in Htt138-transfected cells (Figures 5B–5D). These experiments pointed to TRPC1 as one of the subunits of Isoc channels activated in response to Htt-138Q expression in SK-N-SH cells and inhibited by EVP4593. In additional experiments we demonstrated that RNAi-mediated knockdown of TRPC1 subunit in primary mouse MSN cultures causes significant reduction in the amplitude of thapsigargin-evoked SOC currents (data not shown).

To test the hypothesis that EVP4593 blocks TRPC1-supported channels, we transfected SK-N-SH cells with a mouse TRPC1 expression plasmid. Consistent with the known role of TRPC1 (Clapham et al., 2001), Isoc currents were significantly enhanced in TRPC1-transfected SK-N-SH cells, similar in size to Isoc currents in Htt-138Q-transfected cells (Figure 5A). However, the properties of Isoc currents in TRPC1-transfected cells were different from the properties of Isoc currents in Htt-138Q-transfected cells. The shape of the current-voltage relationship in TRPC1-transfected cells was different, with much larger outward current than in Htt138Q-transfected cells (Figure 5C). Even more

strikingly, currents resulting from TRPC1 overexpression were not sensitive to inhibition by EVP4593 (Figures 5B and 5D). From these experiments we concluded that EVP4593 does not target TRPC1 homomeric channels but rather targets heteromeric channels containing TRPC1 as one of the subunits. Western blotting experiments also indicated that the levels of TRPC1 expression remain constant in Htt-138Q-transfected SK-N-SH cells (Figure S2). Future experiments will be required to identify the subunit of SOC channels that is upregulated in Htt-138Q-transfected cells and forms heteromeric channels with TRPC1.

### EVP4593 and Its Active Analogs Protect YAC128 MSN from Glutamate Toxicity

Do EVP4593 and its analogs exert neuroprotective effects in mammalian model of HD? To answer this question we evaluated activity of EVP4593 and its analogs in glutamate toxicity experiments with primary MSN cultures from YAC128 mice. In the previous studies we described that YAC128 MSN are significantly more susceptible to glutamate-induced apoptosis than WT MSN cultures (Tang et al., 2005). The difference between glutamate-induced apoptosis of YAC128 and WT MSN is significant and consistent, providing a quantitative basis for the *in vitro* HD assay. In the previous studies we took an advantage of this experimental system to evaluate potential neuroprotective effects of a number of clinically relevant compounds (Wu et al., 2006, 2008, 2009). As in previous studies we determined that in the absence of glutamate,  $\sim 5\%$ – $15\%$  of neurons were apoptotic in both WT and YAC128 MSN cultures (Figure 6 and Table 2). After addition of  $250$   $\mu\text{M}$  glutamate, the fraction of apoptotic WT MSN was increased to  $30\%$ – $45\%$  and the fraction of apoptotic YAC128 MSN was increased to  $65\%$ – $80\%$  (Figure 6 and Table 2). The potential neuroprotective effects of EVP4593 and its analogs in our experiments were evaluated at  $30$  nM,  $300$  nM, and  $3$   $\mu\text{M}$  concentrations. In all experiments compounds were added to MSN cultures 30 min before addition of glutamate. We found that EVP4593 significantly protected YAC128 MSN from glutamate toxicity at  $30$  nM and  $300$  nM concentrations (Figures 6A and 6B and Table 2). EVP14756 was equally potent, with significant protective effects at  $30$  nM and  $300$  nM concentrations (Table 2). EVP14782 was not effective at  $30$  nM but was protective at  $300$  nM concentration (Table 2). EVP4593, EVP14756, and EVP14782 became cytotoxic when tested in  $3$   $\mu\text{M}$  concentrations (Table 2). The neurons detached in experiments with  $3$   $\mu\text{M}$  of EVP4593 and EVP14782 and data could not be collected, whereas for EVP14756 the toxicity compromised its neuroprotective effect when tested at  $3$   $\mu\text{M}$  concentration (Table 2). EVP14809 was not effective at  $30$  nM and  $300$  nM concentrations, but demonstrated significant neuroprotective effects at  $3$   $\mu\text{M}$  (Figure 6D and Table 2). EVP14808, EVP14810, and EVP14812 were inactive at any concentrations that were tested (Figure 6C and Table 2). From these results we concluded that when tested in YAC128 MSN excitotoxicity model, EVP4593, EVP14756, and EVP14782 exhibited neuroprotective effects in nanomolar concentrations, EVP14809 was active in micromolar concentration, and EVP14808, EVP14810, and EVP14812 were inactive (Table 1).

Our electrophysiological data suggested that EVP4593 inhibits TRPC1-supported SOC currents and that TRPC1-supported



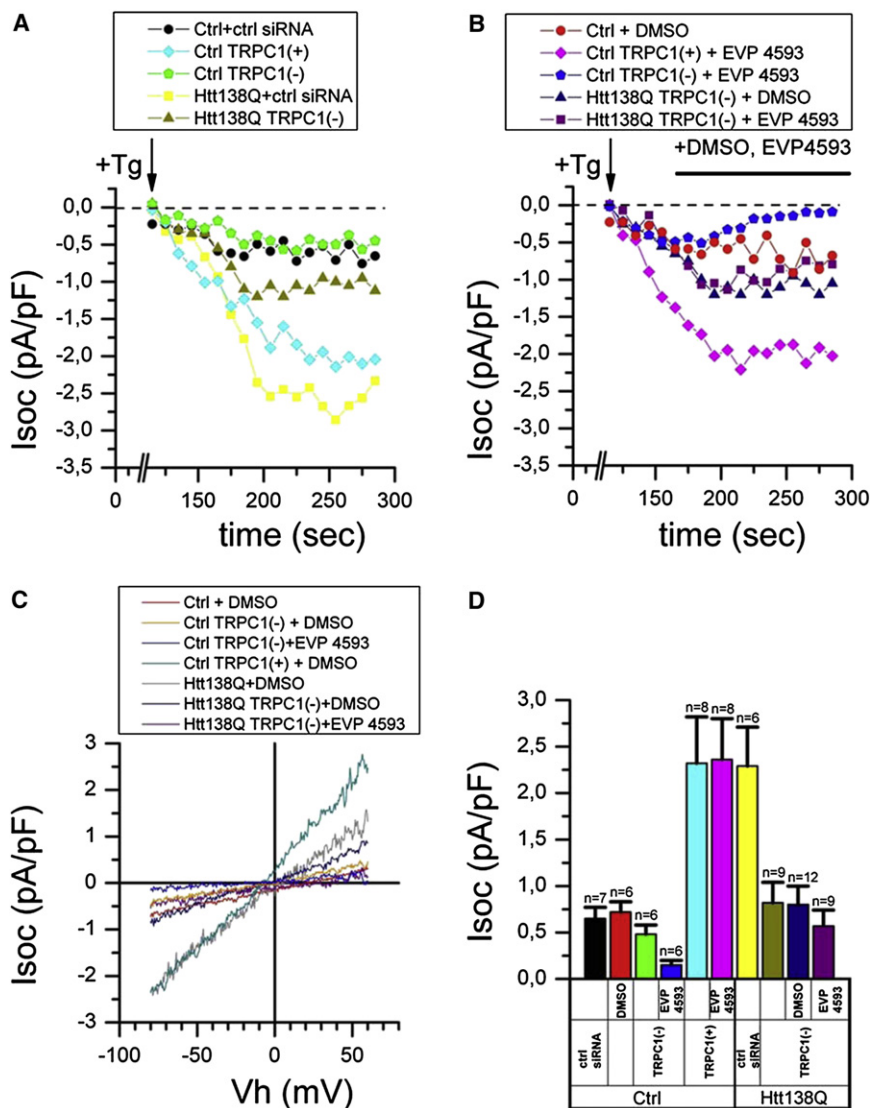


**Figure 5. TRPC1 Supports Isoc Currents in SK-N-SH Cells Transfected with Htt-138Q**

(A) The amplitude of Isoc currents recorded in whole-cell experiments is shown as a function of time after application of 1  $\mu$ M Tg (indicated by arrow) to SK-N-SH cells transiently transfected with scrambled siRNA (Ctrl+ctrl siRNA, black circles), to SK-N-SH cells transiently transfected with TRPC1 plasmid (Ctrl TRPC1+, cyan rhombs), to SK-N-SH cells transiently transfected with TRPC1-RNAi (Ctrl TRPC1-, green pentagons), to SK-N-SH cells transiently cotransfected with Htt-138Q and scrambled siRNA (yellow squares) or to SK-N-SH cells cotransfected with Htt-138Q and TRPC1-RNAi (dark yellow triangles).

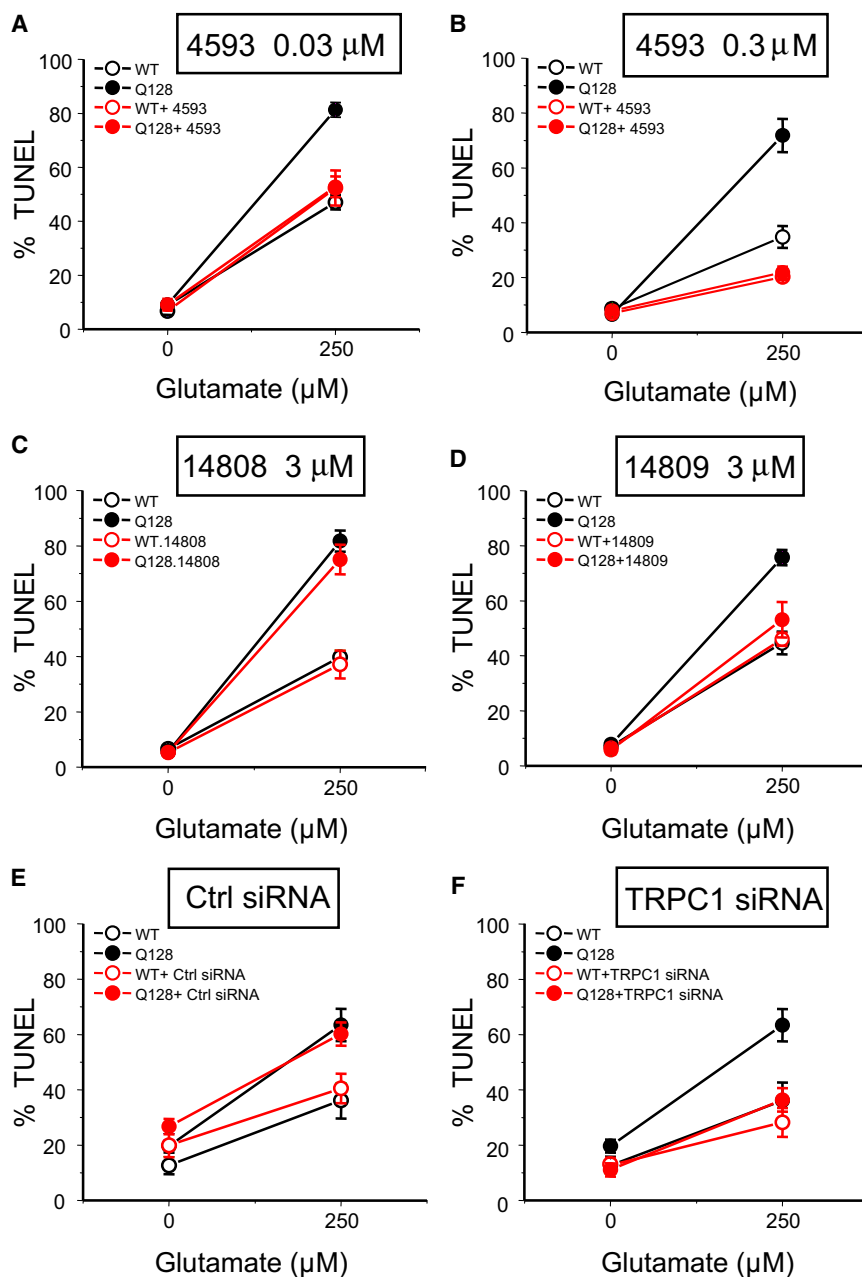
(B) The amplitude of Isoc currents recorded in whole-cell experiments are shown as a function of time after application of 1  $\mu$ M Tg (indicated by arrow) to nontransfected SK-N-SH cells treated with DMSO (Ctrl, red circles), to SK-N-SH cells transiently transfected with TRPC1 and treated with 300 nM EVP4593 (Ctrl TRPC1+, pink rhombs), to SK-N-SH cells transiently transfected with TRPC1-RNAi and treated with 300 nM EVP4593 (Ctrl TRPC1-, blue pentagons), to SK-N-SH cells cotransfected with Htt-138Q and TRPC1-RNAi and treated with DMSO (navy triangles) or to SK-N-SH cells cotransfected with Htt-138Q and TRPC1-RNAi and treated with 300 nM EVP4593 (purple squares). The times of EVP4593 and DMSO applications are shown above the Isoc plot. On (A) and (B) the amplitude of the Isoc currents for all groups of cells was measured every 10 s at -80 mV test potential. Data from representative experiments are shown for each group of cells.

(C) The average current-voltage relationships recorded after full development of Isoc in nontransfected SK-N-SH cells (Ctrl, red trace), in SK-N-SH cells transfected with TRPC1-RNAi and treated with DMSO (yellow trace) or 300 nM EVP4593 (blue trace), in SK-N-SH cells transfected with Htt-138Q and treated with DMSO (black trace), in SK-N-SH cells transfected with TRPC1 and treated with DMSO (gray trace), in SK-N-SH cells cotransfected with Htt-138Q and TRPC1-RNAi and treated with DMSO (navy trace), and in SK-N-SH cells cotransfected with Htt-138Q and TRPC1-RNAi and treated with 300 nM EVP4593 (purple trace). Each trace is an average based on a number of experiments indicated in (D).

(D) The average Isoc amplitude in SK-N-SH cells transfected with scrambled siRNA, in nontransfected SK-N-SH cells treated with DMSO, in SK-N-SH cells transfected with TRPC1-RNAi with and without treatment with 300 nM EVP4593, in SK-N-SH cells transfected with TRPC1-cDNA with and without treatment with 300 nM EVP4593, in SK-N-SH cells cotransfected with Htt-138Q and scrambled siRNA, and in SK-N-SH cells cotransfected with Htt-138Q and TRPC1-RNAi untreated, treated with DMSO or treated with 300 nM EVP4593. For all groups of cells Isoc amplitude was determined at -80 mV test potential and plotted as mean  $\pm$  SE (n = number of experiments). See also Figure S2.

SOC currents are upregulated in response to mutant Htt<sup>EXD</sup> expression (Figure 5). To confirm that neuroprotective effects of EVP compounds are indeed due to inhibition of TRPC1-supported SOC currents, we evaluated neuroprotective effects of TRPC1 RNAi knockdown in YAC128 MSN cultures. In these experiments, expression of mouse TRPC1 was suppressed by application of Dicer-mediated approach. The mixture of siRNA (25–27 nt in size) targeting mouse TRPC1 was generated as described in Experimental Procedures and transfected into WT and YAC128 MSN at second day in vitro (DIV2) together with nontargeting siRNA. In parallel experiments the cells were treated

with transfection reagent (PEI) alone or together with nontargeting siRNA (Ctrl siRNA). In the absence of glutamate, ~10%–25% of neurons were apoptotic in both WT and YAC128 MSN cultures (Figures 6E and 6F and Table 2) in these experiments. The fractions of apoptotic WT and YAC128 MSN treated with nontargeting siRNA increased slightly as a result of transfection procedure (Figure 6E and Table 2), but they were not significantly different from those of WT and YAC128 MSN treated with the transfection reagent alone (Figure 6E and Table 2). After addition of 250  $\mu$ M glutamate, the fraction of apoptotic WT MSN in transfection reagent control was increased to 30%–40% and the



fraction of apoptotic YAC128 MSN in transfection reagent control was increased to ~65% (Figures 6E and 6F and Table 2). The results obtained in cells with nontargeting siRNA were identical to results in cells exposed to transfection reagent alone (Figure 6E and Table 2). In contrast, YAC128 MSN treated with TRPC1 siRNA were significantly protected from glutamate-induced apoptosis when compared to transfection reagent control (Figure 6F and Table 2). The fraction of apoptotic WT MSN treated with TRPC1 siRNA was also slightly decreased, but effect was not significant when compared to transfection reagent control (Figure 6F and Table 2). From these experiments we concluded that RNAi-mediated knockdown of TRPC1 subunit protects YAC128 MSN neurons from glutamate-induced apoptosis.

phenotype, we developed a medium-throughput screening platform for discovery of potential HD therapeutics.

We used the developed screening platform to screen a library of quinazoline-derived compounds and after secondary round of screening identified a compound EVP4593 as a potent hit (Figures 1A and 1B). The same compound has been previously isolated as an inhibitor of PMA/PHA-induced NF- $\kappa$ B pathway activation in Jurkat cells (Tobe et al., 2003b). In our studies we compared a relative efficacy of EVP4593 and its six structure-related analogs (Figure 1C) in *Drosophila* HD climbing assay and PMA/PHA-induced NF- $\kappa$ B activation assay in Jurkat cells. We observed an excellent correlation between relative potencies demonstrated by all seven compounds in these assays

### Figure 6. Compounds from EVP4593 Series or Knockdown of TRPC1 Protect YAC128 MSNs from Glutamate-Induced Apoptosis

The fraction of TUNEL-positive nuclei is plotted against glutamate concentration for MSN from WT (open circles) and YAC128 (YAC, filled circles) mice. The results in the absence (black symbols) and presence (red symbols) of compounds or treatments are compared. The data are shown for (A) 0.03  $\mu$ M of EVP4593; (B) 0.3  $\mu$ M of EVP4593; (C) 3  $\mu$ M of EVP14808; (D) 3  $\mu$ M of EVP14809; (E) treatment with nontargeting RNAi reagent; and (F) treatment with TRPC1 RNAi. In experiments shown in (A–D) the compounds were added 30 min before the application of glutamate. In experiments shown in (E) and (F) neurons were transfected by RNAi at DIV2–4. For each data point the fraction of TUNEL-positive nuclei is shown as mean  $\pm$  SE ( $n = 6$ –8 microscopic fields, 100–300 MSN per field).

### DISCUSSION

In this study, we utilized a phenotypic drug screening platform based on a *Drosophila* transgenic HD model to search for potential HD therapeutics. *Drosophila* has been widely used to model HD and other polyglutamine expansion disorders, revealing several conserved cellular pathways important for pathogenesis (Marsh et al., 2009). In several previous studies pharmacological agents alleviated phenotypes developed by *Drosophila* HD models (Desai et al., 2006; Ravikumar et al., 2004; Steffan et al., 2001). The *Drosophila* HD model used in our study expressed first four exons of human Huntingtin with 128Q expansion under control of an inducible promoter (Al-Ramahi et al., 2006). After induction of Htt-128Q transgene expression in the nervous system, the HD flies developed progressive motor phenotype that can be quantified by using automated climbing assay (Figure 1A). By taking advantage of this reproducible

(Figure 1D and Table 1). Several previous studies suggested that NF- $\kappa$ B pathway might play a direct role in HD pathogenesis. Inhibition of NF- $\kappa$ B activity decreased the striatal lesion in acute excitotoxicity model (Nakai et al., 2000; Qin et al., 1998, 2001). NF- $\kappa$ B activation has been observed in PC12 cells transfected with mutant Huntingtin construct, in R6/2 transgenic HD mice and in HD knock-in mice (Khoshnan et al., 2004; Sugars et al., 2004). The mutant huntingtin has been shown to bind IKK, enhancing IKK activity (Khoshnan et al., 2004). The Htt<sup>exp</sup>-mediated cell death in HEK293 cells and striatal slices can be rescued by blocking IKK activity (Khoshnan et al., 2004). Recent studies revealed that IKK can phosphorylate Htt directly and affect its turnover rate (Thompson et al., 2009). All these results suggest that inhibition of NF- $\kappa$ B pathway may provide a potential approach for neuroprotection in HD (Chu et al., 2007).

However, further examination of isolated compounds indicated that the inhibition of NF- $\kappa$ B pathway is not likely to be directly responsible for the beneficial effects observed in experiments with transgenic HD flies. Structurally unrelated potent IKK and NF- $\kappa$ B inhibitor BMS-345541 was not effective in the climbing assay with HD flies (Figure 1D). Similarly negative results were obtained in experiments with several additional IKK inhibitors that were tested (data not shown). In contrast to the fully potent inhibitor BMS-345541, EVP4593 and its active analogs acted as partial antagonists of NF- $\kappa$ B pathway (Figure S1), consistent with indirect mode of action of these compounds. Moreover, EVP4593 failed to block IKK or PKC directly or exhibit any kinase inhibitory activity in a variety of screening platforms (data not shown). Based on this analysis we hypothesized that EVP4593 may act by inhibiting SOC, which is critical for PMA/PHA-induced NF- $\kappa$ B activation in Jurkat cells. Indeed, it has been previously reported that EVP4593 can inhibit SOC in experiments with SH-5Y5 cells (Choi et al., 2006). In a series of Ca<sup>2+</sup> imaging and electrophysiological experiments we demonstrated that SOC pathway is upregulated in primary MSN neurons from YAC128 transgenic HD mice (Figure 2) and in SK-N-SH human neuroblastoma cells transfected with Htt-138Q expression plasmid (Figure 4). The upregulation of SOC pathway was specifically induced by Htt<sup>exp</sup> and did not occur in SK-N-SH cells transfected with Htt-15Q plasmid (Figure 4). Previous studies demonstrated that the mutant Htt<sup>exp</sup> affects Ca<sup>2+</sup> signaling in MSN by increasing the sensitivity of InsP<sub>3</sub>R1 to InsP<sub>3</sub> (Tang et al., 2003), by potentiating function of NR2B-containing NMDAR (Chen et al., 1999; Fan et al., 2007; Milnerwood and Raymond, 2007; Sun et al., 2001; Zeron et al., 2002; Zhang et al., 2008), and by destabilizing mitochondrial Ca<sup>2+</sup> handling (Choo et al., 2004; Panov et al., 2002). The increase in SOC pathway activity observed in our experiments (Figure 2 and Figure 4) may be a direct result of Htt<sup>exp</sup> expression or may correspond to a compensatory response of the cells to destabilized Ca<sup>2+</sup> signaling. Future studies will be required to address this issue.

Consistent with the previous results (Choi et al., 2006), we demonstrated that EVP4593 effectively inhibited SOC pathway in YAC128 MSN (Figure 2 and Figure 3) and in SK-N-SH cells transfected with Htt-138Q (Figure 4). The inactive analog EVP14808 failed to inhibit SOC pathway in either experimental system (Figures 2–4). Interestingly, EVP4593 was much less potent in inhibiting SOC in WT MSN (Figure 2) or in nontransfected SK-N-SH cells (Figure 4). These results indicate that the

target of EVP4593 is upregulated in neuronal cells in response to mutant Htt<sup>exp</sup> expression. In our studies we observed an excellent correlation between ability of compounds in this series to alleviate phenotype of transgenic HD flies in the climbing assay, to inhibit PMA/PHA-induced NF- $\kappa$ B activation in Jurkat cells and to block SOC in neuronal cells expressing Htt<sup>exp</sup> (Table 1).

The molecular composition of neuronal SOC pathway is poorly understood, with potential components that include members of mammalian Trp family and Orai1 channels (Berna-Erro et al., 2009; Gruszczynska-Biegala et al., 2011; Hasan and Venkiteswaran, 2010; Putney, 2003; Venkiteswaran and Hasan, 2009). The current-voltage relationship of Isoc current in Htt138Q-transfected SK-N-SH cells (Figure 4B) was consistent with relatively nonselective Ca<sup>2+</sup> channels such as Trp channels and not with highly-selective Ca<sup>2+</sup> channels such as Orai1. In our experiments, we demonstrated that RNAi-mediated knockdown of TRPC1 subunit significantly reduced the size of Isoc currents in Htt-138Q-transfected SK-N-SH cells (Figure 5) and in primary mouse MSN neurons (data not shown). We further demonstrated that RNAi-mediated knockdown of TRPC1 occluded ability of EVP4593 to block Isoc currents in Htt138-transfected SK-N-SH cells (Figure 5). From these experiments we concluded that TRPC1 is likely to be one of the subunit of SOC channels upregulated in response to Htt-138Q expression and inhibited by EVP4593. However, EVP4593 failed to inhibit Isoc currents supported by overexpressed TRPC1 (Figure 5). From these experiments, we concluded that EVP4593 does not target TRPC1 homomeric channels but rather targets heteromeric channels containing TRPC1 as one of the subunits. Consistent with this hypothesis, we found that the levels of TRPC1 expression remain constant in Htt-138Q-transfected SK-N-SH cells (Figure S2). Future experiments will be required to identify the subunit of SOC that is upregulated in YAC128 MSNs and in Htt-138Q-transfected cells and forms heteromeric channels with TRPC1.

These experiments suggested that the channels containing TRPC1 subunit might play a significant role in pathogenesis of HD. TRPC1 channels have been previously implicated in excitotoxic cell death of hippocampal neurons (Narayanan et al., 2008). Our conclusions are further supported by recent genetic studies. By using the same fly HD model and climbing assay as used in our study (Figure 1A) it was recently demonstrated that knockout of TRP subunit in *Drosophila* resulted in clear beneficial effects (Al-Ramahi et al., 2010). Our conclusion is also consistent with emerging role played by Trp family members in variety of neurological disorders (Selvaraj et al., 2010; Yamamoto et al., 2007). Mutations in TRPML1 channels cause lysosomal storage neurodegenerative disorder mucopolisaccharidosis type IV (Slaugenhaupt, 2002; Venkatachalam et al., 2008). Recent studies reported that point mutations in TRPV4 channels are linked to hereditary motor and sensor neuropathies in humans (Auer-Grumbach et al., 2010; Deng et al., 2010; Landoure et al., 2010) and the gain-of-function point mutation in TRPC3 channel causes loss of cerebellar Purkinje neurons in the *moonwalker* mice (Becker et al., 2009). A potential importance of Trp channels in Parkinson's disease (PD) and in Alzheimer's disease (AD) has been also been previously discussed (Selvaraj et al., 2010; Yamamoto et al., 2007).

**Table 2. Effects of Drugs and Treatments on Glutamate-Induced Apoptosis in WT and YAC128 MSN**

EVP Compound (conc) <sup>a</sup>	WT (% TUNEL-positive)		YAC128 (% TUNEL-positive)	
	0 $\mu$ M Glutamate	250 $\mu$ M Glutamate	0 $\mu$ M Glutamate	250 $\mu$ M Glutamate
<b>4593</b>				
0.03 $\mu$ M	6.75 $\pm$ 1.40 (8.98 $\pm$ 2.20)	52.37 $\pm$ 6.51 (47.07 $\pm$ 2.69)	9.12 $\pm$ 2.20 (9.09 $\pm$ 1.69)	52.81 $\pm$ 3.85 <sup>b</sup> (81.30 $\pm$ 2.76)
0.3 $\mu$ M	6.91 $\pm$ 1.50 (8.65 $\pm$ 1.68)	20.28 $\pm$ 1.22 <sup>b</sup> (34.84 $\pm$ 3.98)	7.88 $\pm$ 1.61 (6.55 $\pm$ 0.78)	21.86 $\pm$ 2.20 <sup>b</sup> (71.89 $\pm$ 6.05)
3.0 $\mu$ M	—	—	—	—
<b>14756</b>				
0.03 $\mu$ M	7.49 $\pm$ 2.16 (12.38 $\pm$ 2.98)	36.68 $\pm$ 4.24 (40.70 $\pm$ 5.13)	8.08 $\pm$ 1.35 (7.96 $\pm$ 1.07)	48.94 $\pm$ 6.97 <sup>b</sup> (83.99 $\pm$ 3.61)
0.3 $\mu$ M	6.89 $\pm$ 0.75 (7.85 $\pm$ 1.19)	31.99 $\pm$ 4.33 (39.55 $\pm$ 3.49)	6.78 $\pm$ 1.93 (8.32 $\pm$ 1.28)	26.70 $\pm$ 4.14 <sup>b</sup> (67.96 $\pm$ 5.69)
3.0 $\mu$ M	16.43 $\pm$ 1.35 (7.85 $\pm$ 1.19)	31.62 $\pm$ 5.27 (39.55 $\pm$ 3.49)	12.13 $\pm$ 1.93 (8.32 $\pm$ 1.28)	54.71 $\pm$ 3.77 (67.96 $\pm$ 5.69)
<b>14782</b>				
0.03 $\mu$ M	5.59 $\pm$ 1.01 (12.38 $\pm$ 2.98)	34.84 $\pm$ 3.51 (40.70 $\pm$ 5.13)	8.40 $\pm$ 1.62 (7.96 $\pm$ 1.07)	75.09 $\pm$ 5.99 (83.99 $\pm$ 3.61)
0.3 $\mu$ M	6.25 $\pm$ 2.00 (8.65 $\pm$ 1.68)	17.88 $\pm$ 1.50 <sup>b</sup> (34.84 $\pm$ 3.98)	6.01 $\pm$ 1.14 (6.55 $\pm$ 0.78)	30.34 $\pm$ 3.33 <sup>b</sup> (71.89 $\pm$ 6.05)
3.0 $\mu$ M	—	—	—	—
<b>14808</b>				
0.03 $\mu$ M	8.76 $\pm$ 1.22 (8.98 $\pm$ 2.20)	57.43 $\pm$ 5.64 (47.07 $\pm$ 2.69)	7.10 $\pm$ 1.16 (9.09 $\pm$ 1.69)	78.33 $\pm$ 5.88 (81.30 $\pm$ 2.76)
0.3 $\mu$ M	5.75 $\pm$ 1.30 (7.85 $\pm$ 1.19)	39.46 $\pm$ 4.19 (39.55 $\pm$ 3.49)	10.77 $\pm$ 2.71 (8.32 $\pm$ 1.28)	56.08 $\pm$ 4.72 (67.96 $\pm$ 5.69)
3.0 $\mu$ M	5.26 $\pm$ 0.83 (6.64 $\pm$ 1.32)	37.18 $\pm$ 5.04 (39.77 $\pm$ 2.56)	5.38 $\pm$ 0.84 (5.45 $\pm$ 1.07)	75.15 $\pm$ 5.35 (81.80 $\pm$ 3.84)
<b>14809</b>				
0.03 $\mu$ M	14.93 $\pm$ 2.00 (12.38 $\pm$ 2.98)	42.95 $\pm$ 4.63 (40.70 $\pm$ 5.13)	9.31 $\pm$ 2.49 (7.96 $\pm$ 1.07)	70.96 $\pm$ 5.21 (83.99 $\pm$ 3.61)
0.3 $\mu$ M	8.76 $\pm$ 3.15 (8.65 $\pm$ 1.68)	39.39 $\pm$ 4.48 (34.84 $\pm$ 3.98)	5.97 $\pm$ 0.80 (6.55 $\pm$ 0.78)	61.37 $\pm$ 9.22 (71.89 $\pm$ 6.05)
3.0 $\mu$ M	6.51 $\pm$ 1.70 (6.98 $\pm$ 0.95)	46.05 $\pm$ 2.40 (44.71 $\pm$ 4.12)	5.82 $\pm$ 1.56 (7.80 $\pm$ 1.56)	53.15 $\pm$ 6.42 <sup>b</sup> (75.75 $\pm$ 2.80)
<b>14810</b>				
0.03 $\mu$ M	8.31 $\pm$ 1.17 (7.59 $\pm$ 1.51)	41.95 $\pm$ 5.49 (35.29 $\pm$ 3.89)	7.72 $\pm$ 0.96 (6.97 $\pm$ 1.71)	71.98 $\pm$ 5.16 (70.24 $\pm$ 5.17)
0.3 $\mu$ M	9.37 $\pm$ 1.59 (8.98 $\pm$ 2.20)	52.73 $\pm$ 4.49 (47.07 $\pm$ 2.69)	8.49 $\pm$ 2.08 (9.09 $\pm$ 1.69)	79.37 $\pm$ 3.08 (81.30 $\pm$ 2.76)
3.0 $\mu$ M	5.12 $\pm$ 0.62 (7.59 $\pm$ 1.51)	33.57 $\pm$ 4.88 (35.29 $\pm$ 3.89)	6.62 $\pm$ 1.06 (6.97 $\pm$ 1.71)	64.63 $\pm$ 4.41 (70.24 $\pm$ 5.17)
<b>14812</b>				
0.03 $\mu$ M	5.95 $\pm$ 1.59 (7.59 $\pm$ 1.51)	40.85 $\pm$ 4.61 (35.29 $\pm$ 3.89)	6.10 $\pm$ 1.16 (6.97 $\pm$ 1.71)	68.50 $\pm$ 4.62 (70.24 $\pm$ 5.17)
0.3 $\mu$ M	8.97 $\pm$ 1.71 (10.67 $\pm$ 2.10)	39.16 $\pm$ 5.34 (35.90 $\pm$ 4.11)	9.15 $\pm$ 1.76 (9.28 $\pm$ 1.13)	73.68 $\pm$ 5.29 (70.27 $\pm$ 5.13)
3.0 $\mu$ M	8.06 $\pm$ 1.75 (7.59 $\pm$ 1.51)	39.36 $\pm$ 3.48 (35.29 $\pm$ 3.89)	6.14 $\pm$ 0.61 (6.97 $\pm$ 1.71)	68.48 $\pm$ 6.31 (70.24 $\pm$ 5.17)
Ctrl siRNA	19.93 $\pm$ 4.24 (12.69 $\pm$ 3.19)	40.55 $\pm$ 5.35 (36.16 $\pm$ 6.51)	26.75 $\pm$ 2.77 (19.68 $\pm$ 2.34)	60.22 $\pm$ 4.19 (63.47 $\pm$ 5.87)

Table 2. Continued

EVP Compound (conc) <sup>a</sup>	WT (% TUNEL-positive)		YAC128 (% TUNEL-positive)	
	0 $\mu$ M Glutamate	250 $\mu$ M Glutamate	0 $\mu$ M Glutamate	250 $\mu$ M Glutamate
TRPC1 siRNA	12.72 $\pm$ 2.75 (12.69 $\pm$ 3.19)	28.27 $\pm$ 5.20 (36.16 $\pm$ 6.51)	11.07 $\pm$ 2.40 (19.68 $\pm$ 2.34)	36.39 $\pm$ 4.24 <sup>b</sup> (63.47 $\pm$ 5.87)

<sup>-</sup> toxic, total number of cells are much less than control; Conc, concentration; MSN, medium spiny neurons; TUNEL, terminal deoxynucleotidyl transferase dUTP nick end labeling; WT, wild-type.

<sup>a</sup> In EVP compound experiment, the number in parenthesis is the untreated control cells in the same batch of MSN culture. In siRNA experiment, the number is the control cells treated with transfection reagent in the same batch of culture.

<sup>b</sup>  $p < 0.05$ , compared with control cells and show protective effect.

To further evaluate therapeutic potential of identified compounds, we evaluated neuroprotective effects of these compounds in glutamate toxicity model with YAC128 primary MSN cultures. In the previous studies we utilized the same experimental system to evaluate potential neuroprotective effects of a number of clinically relevant compounds (Wu et al., 2006, 2008, 2009). Based on the obtained results (Figure 6 and Table 2), we concluded that EVP4593, EVP14756, and EVP14782 exhibited neuroprotective effects in nanomolar concentrations, EVP14809 was active in micromolar concentration and EVP14808, EVP14810, and EVP14812 were inactive. Overall, there was an excellent correlation between neuroprotective effects of these compounds in YAC128 MSN glutamate toxicity model, ability of these compounds to block SOC and PMA/PHA-induced NF- $\kappa$ B activation, and efficacy in the climbing assay with HD flies (Table 1). We further established that Dicer RNAi-mediated knockdown of mouse TRPC1 subunit in YAC128 MSN results in significant neuroprotective effect in glutamate toxicity model (Figure 6F and Table 2). These results further supported hypothesis that TRPC1-mediated SOC channels can be considered as a potential target for developing novel HD therapeutics.

## SIGNIFICANCE

The importance of store-operated  $Ca^{2+}$  entry (SOC) pathway in neuronal function is poorly understood (Hasan and Venkiteswaran, 2010; Putney, 2003). However, potential role of neuronal SOC pathway in pathological conditions has been suggested based on studies with experimental models of AD (Herms et al., 2003; Leissring et al., 2000; Yamamoto et al., 2007; Yoo et al., 2000), PD (Bollimuntha et al., 2005; Selvaraj et al., 2009), cerebral ischemia (Berna-Erro et al., 2009), and excitotoxicity (Narayanan et al., 2008). Our study together with the recent meeting report (Al-Ramahi et al., 2010) provide the first evidence that the SOC pathway may also play an important role in HD. In experiments with transgenic *Drosophila* HD model, cultured MSN neurons from YAC128 HD mouse model and SK-N-SH human neuroblastoma cells transfected with mutant Htt expression constructs we demonstrated that SOC pathway is upregulated in HD neurons. Moreover, we demonstrated that pharmacological inhibition or genetic knockdown of TRPC1-mediated SOC pathway protects HD neurons from toxicity. These results provide further support to the emerging hypothesis that deranged neuronal  $Ca^{2+}$  signaling plays a key role in

HD pathogenesis (Bezprozvanny, 2009). Based on our results, we concluded that the TRPC1-mediated SOC pathway constitute a novel target for potential HD treatment. In addition, we identified a number of quinazoline-derived compounds (EVP4593, EVP14756, and EVP14782) (Figure 1C) with ability to block neuronal SOC. These compounds can be used to dissect role of neuronal SOC in neuronal physiology. The same compounds may also provide leads for developing a novel class of therapeutic agents for treatment of HD and possibly other neurodegenerative disorders. Testing these compounds in mouse models of HD and other neurodegenerative disorders will help to evaluate future therapeutic potential of these molecules.

## EXPERIMENTAL PROCEDURES

### Compounds

Glutamate was from Tocris. Fura-2/AM and Trichostain A (TSA) were purchased from Sigma. EVP4593 (6-amino-4-(4-phenoxyphenethyl-amino)quinazoline), EVP14782 (6-amino-4-(4-ethoxyphenethylamino)quinazoline), EVP14756 (6-amino-4-(4-n-pentyloxyphenethylamino)quinazoline), EVP14809 (4-(4-chlorophenethylamino)-6-nitroquinazoline), EVP14810 (4-(3-(phenyl)propylamino)quinazoline), EVP14812 (4-(4-acetamido)-phenethylamino-6-amino-quinazoline), and EVP14808 (6-amino-4-(2-(3-pyridyl)ethylamino)-quinazoline) were previously described (Tobe et al., 2003a, 2003b). The compounds were synthesized by standard organic chemistry methods (EnVivo Inc). The structures of generated compounds were confirmed by mass spectrometry and NMR analysis (EnVivo Inc). BMS-345541 was purchased from Calbiochem (Cat. No. 401480). All compounds were dissolved in DMSO as 10 mM stocks for use in animal and cellular assays.

### *Drosophila* Climbing Assay

*Drosophila* stocks and crosses were maintained using standard procedures at 25°C, 70% relative humidity. The transgenic mutant Huntington line, *C(1)DX y<sup>1</sup> w<sup>1118</sup> f<sup>1</sup> P{w<sup>+</sup> HS-hid<sup>+</sup>}18a/P{w<sup>+</sup> mC Act5C-GFP}JMR3; P{UAS-mhtt128Q}F27B* and the pan-neuronal driver, *elav-GAL4<sup>C155</sup>/Y, P{w<sup>+</sup> HS-hid<sup>+</sup>}* were used to generate HD flies, *elav-GAL4<sup>C155</sup>/P{w<sup>+</sup> mC Act5C-GFP}JMR3; P{UAS-mhtt128Q}F27B/+* expressing first four exons of human Htt-128Q in the nervous system of the flies as previously described (Al-Ramahi et al., 2006). The motor function of HD flies or control flies (*UAS-LacZ* driven by *elav-GAL4* driver) were automatically monitored using tracking device to measure the speed of upward climbing within 7.5 s after dropping the flies to the bottom of the tube. This proprietary assay system and screening method have been developed by EnVivo Inc. HD flies were treated with compounds dissolved in a proprietary medium in concentration at 400  $\mu$ M in the presence of 1% DMSO. After induction of Htt-128Q transgene fragment expression, the flies were dosed daily with testing compounds and motor assays were performed. For each compound treatment, 10 flies were dispensed into each tube and assayed in triplicate. To quantify the effect of the tested compounds the difference in the average climbing speed was calculated between the groups of transgenic HD flies treated with the compound of interest and the groups

treated with 1% DMSO. The difference was normalized to the standard deviation in the climbing speed determined for the entire DMSO-treated group, yielding a quantitative measure of the effect size. Statistical models indicated that in the assay conditions used (10 flies per tube, 16 tubes for one treatment and three independent experiments), effect size of 0.5 corresponds to  $p$  value of 0.03 and the effect size of 0.8 has a  $p$  value in the range between 0.03 and 0.003. Compounds showing an effect size  $>0.8$  ( $p < 0.003$ ) in the early time points (days 1–7) or an effect size  $>1.2$  in the late time points (days 8–10) after three repeated assays were qualified as potential hits and evaluated further.

#### NF- $\kappa$ B Assays

Human Jurkat cells (clone E6-1) were acquired from American Type Culture Collection and cultured in RPMI 1640 media (Invitrogen) supplemented with 10% FBS and 1% PS. The cells were plated at a density of  $2 \times 10^6$  cells/well in 6-well dishes and transiently transfected with  $1 \mu\text{g}/\text{well}$  of *pNF- $\kappa$ B-Luc* (Path Detect NF- $\kappa$ B reporter plasmid, Stratagene) using SuperFect Transfection Reagent (QIAGEN). After transfection, cells were incubated for 18 hr and resuspended in RPMI 1640 medium without penicillin-streptomycin and FBS, resulting in  $1.75 \times 10^5$  cells/well in the 96-well plates. Compounds were added 30 min before the addition of a combination of 50 ng/ml of PMA (P1585, Sigma) and 100  $\mu\text{g}/\text{ml}$  of PHA (L1668, Sigma). The plates were incubated for 6 hr at 37°C and luciferase assays were performed (Bright-Glo Luciferase Assay System, Promega). Cell viability was measured by using MTS assay (Promega) to determine the compound toxicity.

#### SOC Measurements

YAC128 mice (FVBN/NJ background strain) (Slow et al., 2003) were obtained from Jackson Labs (stock number 004938). The male YAC128 mice were crossed to WT female FVBN/NJ mice. P1-P2 pups were collected and genotyped by PCR. The primary cultures of MSN were established from YAC128 hemizygotes and WT pups as previously described (Tang et al., 2005). Briefly, striata were dissected, diced, and digested with trypsin. After dissociation, neurons were plated on poly-L-lysine (Sigma) coated, 12 mm round coverslips (Assistant) in Neurobasal-A medium supplemented with 2% B27, 1 mM of glutamine and penicillin-streptomycin (Invitrogen), and kept at 37°C in a 5% CO<sub>2</sub> environment.

Ca<sup>2+</sup> imaging experiments with 10–14 DIV MSN cultures were performed using a DeltaRAM illuminator, an IC-300 camera, and processed by the IMAGEMASTER PRO software (PTI, Photon Technology International) as we previously described (Tang et al., 2005). Briefly, the MSN were loaded with 5  $\mu\text{M}$  of Fura-2 AM for 45 min at 37°C in artificial cerebrospinal fluid containing 140 mM of NaCl, 5 mM of KCl, 1 mM of MgCl<sub>2</sub>, 2 mM of CaCl<sub>2</sub>, and 10 mM of HEPES pH 7.3 (ACSF). Coverslips were mounted onto a recording/perfusion chamber (RC-26G, Warner Instruments) and positioned on the movable stage of an Olympus (Melville) IX-70 inverted microscope. Images at 340 and 380 nm excitation wavelengths were acquired every 2 s and 340/380 Fura-2 image ratio was calculated. To determine SOC activity the cells were incubated in Ca<sup>2+</sup>-free ACSF in the presence of 1  $\mu\text{M}$  SERCA pump inhibitor thapsigargin for 5 min and then transferred back to ACSF containing 2 mM Ca<sup>2+</sup>. The tested compounds were added to the cells 10 min before transfer to 2 mM Ca<sup>2+</sup>.

The manganese (Mn<sup>2+</sup>) quenching experiments were designed based on the published studies (Dadsetan et al., 2008; Yang et al., 2005). In these experiments, the rate of Fura-2 fluorescence quenching in the presence of extracellular Mn<sup>2+</sup> is used as a measure of SOC activity. The Fura-2 fluorescence was measured at isosbestic plot of 360 nm, which is not affected by changes in cytosolic Ca<sup>2+</sup> concentration. For quenching experiments the cells were placed in Ca<sup>2+</sup>-free ACSF and SERCA pump activity was blocked by addition of CPA. The quenching measurements were initiated by addition of 150  $\mu\text{M}$  of Mn<sup>2+</sup> to the extracellular media. Fura-2 fluorescent images were collected at 360 nm excitation wavelength (F<sub>360</sub>) every 6 s. The rate of the F<sub>360</sub> decline due to Fura-2 quenching is proportional to the rate of Mn<sup>2+</sup> entry into the cytosol and was used as an indicator of SOC activity. The tested compounds were added to the cells 5 min after addition of Mn<sup>2+</sup> solution and the rate of Fura-2 quenching was reassessed.

#### Electrophysiological Assays

SK-N-SH human neuroblastoma cells (Cell Culture Collection, Institute of Cytology, St. Petersburg, Russia) were transiently cotransfected with

Htt-15Q or Htt-138Q expression constructs and EGFP plasmid in 3:1 molar ratio as we previously described for MSN cultures (Tang et al., 2003). For TRPC1 knockdown experiments SK-N-SH cells were transiently cotransfected with a mixture of Htt-138Q expression construct, RNAi-TRPC1 plasmid and EGFP plasmid in 3:3:2 molar ratio. For TRPC1 overexpression experiments SK-N-SH cells were transiently cotransfected with a mixture of mouse TRPC1 construct in pcDNA3 expression vector (provided by Dr. Shmuel Muallem, NIH) and EGFP plasmid in 1:1 molar ratio. The RNAi-TRPC1 knockdown plasmid was obtained by cloning the human TRPC1-derived sequence into pSHAG vector and it was kindly provided to us by Dr. Leonidas Tsiokas (University of Oklahoma Health Sciences Center) (Bai et al., 2008). The efficiency of TRPC1 knockdown was confirmed by western blotting of SK-N-SH cellular lysates with anti-TRPC1 polyclonal antibodies (1:200, Alomone Labs, #ACC-010). The transfected cells were identified by GFP fluorescence and the SOC currents were measured 48 hr after transfection using whole-cell recordings as previously described for A431 cells (Gusev et al., 2003). Briefly, whole-cell recordings were performed using an Axopatch 200B patch clamp amplifier (Axon Instruments). Resistance of silyard-coated, fire-polished glass microelectrodes was 3–5 M $\Omega$ . Series resistance was not compensated. The pipette solution contained (in mM) 145 NMDG aspartate, 10 Cs-EGTA, 10 Cs-HEPES pH 7.3, 1.5 MgCl<sub>2</sub>, 4 Na<sub>2</sub>ATP, 0.4 Na<sub>2</sub>GTP, and 4.8 CaCl<sub>2</sub> (pCa 7.0). Extracellular solution contained (in mM) 140 NMDG aspartate, 10 BaCl<sub>2</sub>, 10 Cs-HEPES, 0.01 Tetrodotoxin (Alomone Labs, Israel), 0.01 Nifedipine (Sigma Aldrich, USA) pH 7.3. For the store depletion thapsigargin (1  $\mu\text{M}$ , Sigma Aldrich) was used. During recording the currents were sampled at 5 kHz and filtered digitally at 500 Hz. pClamp6 software suite (Axon Instruments) was used for data acquisition and analysis. In all whole-cell experiments the holding potential was  $-40$  mV. Periodically (once every 5 s) the membrane potential was stepped to  $-100$  mV (for 30 ms) and a 170 ms voltage ramp to  $+70$  mV was applied. Traces recorded before current activation were used as a template for leak subtraction. The recorded currents were normalized to the cell capacitance. Mean value of cell capacitance was  $15 \pm 4$  pF ( $n = 55$ ).

The primary cultures of striatal medium spiny neurons (MSN) were established from WT mice pups (were collected at postnatal days 1–2) as described above for Ca<sup>2+</sup> imaging experiments. Shuttle plasmid construct encoding shRNA against TRPC1 were obtained from Sigma Aldrich (MN\_011643). Lenti-antiTRPC1 viruses were generated by cotransfection of shuttle vector with HIV-1 packaging vector 8.9 and VSVG envelope glycoprotein plasmids into the packaging cell line HEK293T as we previously described (Tang et al., 2009). Lenti-antiTRPC1 virus was added to MSN culture at DIV6 and the whole-cell patch-clamp recordings of currents in cultured DIV10 MSN were performed according to procedures described for SK-N-SH cells with addition of 10 mM glucose to the extracellular solution.

#### YAC128 MSN Glutamate Toxicity Assay

The assay for glutamate-induced cell death was performed with primary WT and YAC128 MSN as we previously described (Tang et al., 2005). The primary cultures were established as described above. Test compounds were added at 14 DIV to WT and YAC128 MSN cultures at the final concentration of 0.03  $\mu\text{M}$ , 0.3  $\mu\text{M}$ , and 3.0  $\mu\text{M}$  from DMSO stocks as indicated. In parallel control experiments the cultures were exposed to 1% DMSO. After 30 min incubation with the test compounds, the MSN were exposed for 7 hr to 250  $\mu\text{M}$  of glutamate added to the culture medium. Immediately after the treatment with glutamate, neurons were fixed for 30 min in 4% formaldehyde plus 4% sucrose in PBS (pH 7.4), permeabilized for 5 min in 0.25% Triton X-100, and stained by using the DeadEnd fluorometric TUNEL System (Promega). Nuclei were counterstained with 5  $\mu\text{M}$  of propidium iodide (PI) (Molecular Probes). Coverslips were extensively washed with PBS and mounted in Mowiol 4-88 (Polysciences). Six to eight randomly chosen microscopic fields containing 100–300 MSN each were manually counted using Olympus IX70 fluorescent microscope. The number of TUNEL-positive neuronal nuclei was calculated as a fraction of PI-positive neuronal nuclei in each microscopic field. The fractions of TUNEL-positive nuclei determined for each microscopic field were averaged and the results are presented as means  $\pm$  SE ( $n =$  number of fields counted).

Dicer-mediated approach was used to achieve siRNA knockdown of TRPC1 in primary MSN cultures by following described procedures (Supnet

et al., 2006). Full-length mouse TRPC1 cDNA was obtained from Open Biosystems (clone ID 8860600) and used as a PCR template to amplify a 300 bp fragment (bp 2102–2401 in mouse TRPC1). T7 promoter sequence was included in the sequence of both forward and reverse primers as follows: FP = TAATACGACTCACTATAGGGTTCCTCTCCAAAGA, RP = TAATACGACTCACTATAGGGTAGAAGTCCGAAAGC. The product of PCR reaction was purified by NucleoSpin Extract II (Clontech) and dsRNA was obtained by T7 polymerase-mediated transcription for 16 hr at 37°C (TurboScript T7 Transcription Kit, Genlantis) followed by DNase I digestion for 15 min at 37°C. dsRNA was purified by lithium chloride precipitation and quantified using NanoDrop 2000c (Thermo Scientific). Four microgram dsRNA and four units of recombinant PowerCut Dicer enzyme (Finnzymes) were combined with PowerCut Dicer Reaction Buffer in a total volume of 20  $\mu$ l. After 16 hr at 37°C, dsRNA was purified on two consecutive RNA purification columns to remove salts and free nucleotides. Described procedure yielded a size-homogeneous population <30 bp dsRNA without contaminating long dsRNA. Concentration of dsRNA was determined by NanoDrop 2000c. The WT and YAC128 MSN cultures were transfected on DIV2–4 by a mixture of 275 ng siRNA-TRPC1 and 1  $\mu$ M Accell fluorescently-labeled nontargeting siRNA reagent (Thermo Scientific Dharmacon) using polyethylenimine (PEI) transfection reagent. The same amount of nontargeting siRNA reagent was used in control transfections (Ctrl-siRNA). In both cases the neuronal transfection efficiency was at least 80%, consistent with the previous studies (Supnet et al., 2006). On DIV14, the MSN were exposed for 7 hr to 250  $\mu$ M of glutamate added to the culture medium and then were fixed and permeabilized as described above. The neurons were stained using In Situ Cell Death Detection Kit, TMR red (Roche). Nuclei were counterstained with 3  $\mu$ M of 4'-6-diamidino-2-phenylindole (DAPI). Six to eight randomly chosen microscopic fields containing 100–300 MSN each were manually counted. The number of TUNEL-positive neuronal nuclei was calculated as a fraction of DAPI-positive neuronal nuclei in each microscopic field. The fractions of TUNEL-positive nuclei determined for each microscopic field were averaged and the results are presented as means  $\pm$  SE (n = number of fields counted).

### Statistical Analysis

All experiments were repeated for at least three times. Data were evaluated for statistical significance by analysis using Sigma Plot t test or one-way ANOVA. Statistical difference was considered to be significant only if  $p < 0.05$ .

### SUPPLEMENTAL INFORMATION

Supplemental Information includes two figures and can be found with this article online at [doi:10.1016/j.chembiol.2011.04.012](https://doi.org/10.1016/j.chembiol.2011.04.012).

### ACKNOWLEDGMENTS

We thank Juan Botas (Baylor University) for generously providing us transgenic mh128 HD flies that were used to generate the stocks in this study, Leonidas Tsiokas (University of Oklahoma Health Sciences Center) for a gift of human TRPC1-RNAi plasmid, Yuemei Li and Huarui Liu for help with maintaining the YAC128 mouse colony and genotyping, Leah Benson for administrative assistance, and Tie-Shan Tang for helpful advice. I.B. is a holder of Carl J. and Hortense M. Thomsen chair in Alzheimer's disease research. The study was supported by EnVivo Inc, CHDI foundation, and the NINDS (R01 NS056224 to I.B.), the Program of Ministry of Science and Education GCs N 14.740.11.0924 (I.B. and E.K.) and N P332 (E.K.), the program of Molecular and Cellular Biology RAS (EK), and Russian Basic Research Foundation 10-04-00956 (E.K.). H.-P.S., L.H., L.D., C.S., M.M., R.C., G.S., M.A., and G.K. are current or former employees and shareholders of EnVivo Inc. This work was supported in part by a contract with EnVivo Inc. I.B. was a paid consultant of EnVivo Inc.

Received: August 16, 2010

Revised: April 5, 2011

Accepted: April 18, 2011

Published: June 23, 2011

### REFERENCES

- Al-Ramahi, I., Kim, E. Sanhueza, M., Diaz, J., and Botas, J. (2010). Screen of genes involved in  $Ca^{2+}$  homeostasis and signaling to identify genetic modifiers and potential therapeutic targets for Huntington's Disease treatment. Paper presented at Society for Neuroscience (San Diego, CA), November 13–17, 2010.
- Al-Ramahi, I., Lam, Y.C., Chen, H.K., de Gouyon, B., Zhang, M., Perez, A.M., Branco, J., de Haro, M., Patterson, C., Zoghbi, H.Y., et al. (2006). CHIP protects from the neurotoxicity of expanded and wild-type ataxin-1 and promotes their ubiquitination and degradation. *J. Biol. Chem.* **281**, 26714–26724.
- Auer-Grumbach, M., Olschewski, A., Papic, L., Kremer, H., McEntagart, M.E., Uhrig, S., Fischer, C., Frohlich, E., Balint, Z., Tang, B., et al. (2010). Alterations in the ankyrin domain of TRPV4 cause congenital distal SMA, scapuloperoneal SMA and HMSN2C. *Nat. Genet.* **42**, 160–164.
- Bai, C.X., Giamarchi, A., Rodat-Despoix, L., Padilla, F., Downs, T., Tsiokas, L., and Delmas, P. (2008). Formation of a new receptor-operated channel by heteromeric assembly of TRPP2 and TRPC1 subunits. *EMBO Rep.* **9**, 472–479.
- Becker, E.B., Oliver, P.L., Glitsch, M.D., Banks, G.T., Achilli, F., Hardy, A., Nolan, P.M., Fisher, E.M., and Davies, K.E. (2009). A point mutation in TRPC3 causes abnormal Purkinje cell development and cerebellar ataxia in moonwalker mice. *Proc. Natl. Acad. Sci. USA* **106**, 6706–6711.
- Berna-Erro, A., Braun, A., Kraft, R., Kleinschnitz, C., Schuhmann, M.K., Stegner, D., Wulsch, T., Eilers, J., Meuth, S.G., Stoll, G., et al. (2009). STIM2 regulates capacitive  $Ca^{2+}$  entry in neurons and plays a key role in hypoxic neuronal cell death. *Sci. Signal.* **2**, ra67.
- Bezprozvanny, I. (2009). Calcium signaling and neurodegenerative diseases. *Trends Mol. Med.* **15**, 89–100.
- Bollimuntha, S., Singh, B.B., Shavali, S., Sharma, S.K., and Ebadi, M. (2005). TRPC1-mediated inhibition of 1-methyl-4-phenylpyridinium ion neurotoxicity in human SH-SY5Y neuroblastoma cells. *J. Biol. Chem.* **280**, 2132–2140.
- Bootman, M.D., Collins, T.J., Mackenzie, L., Roderick, H.L., Berridge, M.J., and Peppiatt, C.M. (2002). 2-aminoethoxydiphenyl borate (2-APB) is a reliable blocker of store-operated  $Ca^{2+}$  entry but an inconsistent inhibitor of InsP3-induced  $Ca^{2+}$  release. *FASEB J.* **16**, 1145–1150.
- Burke, J.R., Pattoli, M.A., Gregor, K.R., Brassil, P.J., MacMaster, J.F., McIntyre, K.W., Yang, X., Iotzova, V.S., Clarke, W., Strnad, J., et al. (2003). BMS-345541 is a highly selective inhibitor of I kappa B kinase that binds at an allosteric site of the enzyme and blocks NF-kappa B-dependent transcription in mice. *J. Biol. Chem.* **278**, 1450–1456.
- Cha, J.H. (2007). Transcriptional signatures in Huntington's disease. *Prog. Neurobiol.* **83**, 228–248.
- Chen, N., Luo, T., Wellington, C., Metzler, M., McCutcheon, K., Hayden, M.R., and Raymond, L.A. (1999). Subtype-specific enhancement of NMDA receptor currents by mutant huntingtin. *J. Neurochem.* **72**, 1890–1898.
- Choi, S., Kim, J.H., Roh, E.J., Ko, M.J., Jung, J.E., and Kim, H.J. (2006). Nuclear factor-kappaB activated by capacitative  $Ca^{2+}$  entry enhances muscarinic receptor-mediated soluble amyloid precursor protein (sAPP $\alpha$ ) release in SH-SY5Y cells. *J. Biol. Chem.* **281**, 12722–12728.
- Choo, Y.S., Johnson, G.V., MacDonald, M., Detloff, P.J., and Lesort, M. (2004). Mutant huntingtin directly increases susceptibility of mitochondria to the calcium-induced permeability transition and cytochrome c release. *Hum. Mol. Genet.* **13**, 1407–1420.
- Chu, C.T., Plowey, E.D., Wang, Y., Patel, V., and Jordan-Sciutto, K.L. (2007). Location, location, location: altered transcription factor trafficking in neurodegeneration. *J. Neuropathol. Exp. Neurol.* **66**, 873–883.
- Clapham, D.E., Runnels, L.W., and Strubing, C. (2001). The TRP ion channel family. *Nat. Rev. Neurosci.* **2**, 387–396.
- Dadsetan, S., Zakharova, L., Molinski, T.F., and Fomina, A.F. (2008). Store-operated  $Ca^{2+}$  influx causes  $Ca^{2+}$  release from the intracellular  $Ca^{2+}$  channels that is required for T cell activation. *J. Biol. Chem.* **283**, 12512–12519.
- Deng, H.X., Klein, C.J., Yan, J., Shi, Y., Wu, Y., Fecto, F., Yau, H.J., Yang, Y., Zhai, H., Siddique, N., et al. (2010). Scapuloperoneal spinal muscular atrophy

- and CMT2C are allelic disorders caused by alterations in TRPV4. *Nat. Genet.* **42**, 165–169.
- Desai, U.A., Pallos, J., Ma, A.A., Stockwell, B.R., Thompson, L.M., Marsh, J.L., and Diamond, M.I. (2006). Biologically active molecules that reduce polyglutamine aggregation and toxicity. *Hum. Mol. Genet.* **15**, 2114–2124.
- Fan, M.M., Fernandes, H.B., Zhang, L.Y., Hayden, M.R., and Raymond, L.A. (2007). Altered NMDA receptor trafficking in a yeast artificial chromosome transgenic mouse model of Huntington's disease. *J. Neurosci.* **27**, 3768–3779.
- Gil, J.M., and Rego, A.C. (2008). Mechanisms of neurodegeneration in Huntington's disease. *Eur. J. Neurosci.* **27**, 2803–2820.
- Gruszczynska-Biegala, J., Pomorski, P., Wisniewska, M.B., and Kuznicki, J. (2011). Differential roles for STIM1 and STIM2 in store-operated calcium entry in rat neurons. *PLoS ONE* **6**, e19285.
- Gusev, K., Glouchankova, L., Zubov, A., Kaznacheyeva, E., Wang, Z., Bezprozvanny, I., and Mozhayeva, G.N. (2003). The store-operated calcium entry pathways in human carcinoma A431 cells: functional properties and activation mechanisms. *J. Gen. Physiol.* **122**, 81–94.
- Hasan, G., and Venkiteswaran, G. (2010). The enigma of store-operated calcium entry in neurons: answers from the *Drosophila* flight circuit. *Front Neural Circuits* **4**, 10.
- Hems, J., Schneider, I., Dewachter, I., Caluwaerts, N., Kretschmar, H., and Van Leuven, F. (2003). Capacitive calcium entry is directly attenuated by mutant presenilin-1, independent of the expression of the amyloid precursor protein. *J. Biol. Chem.* **278**, 2484–2489.
- Huntington's Disease Collaborative Research Group. (1993). A novel gene containing a trinucleotide repeat that is expanded and unstable on Huntington's disease chromosomes. *Cell* **72**, 971–983.
- Huntington Study Group. (2006). Tetrabenazine as antichorea therapy in Huntington disease: a randomized controlled trial. *Neurology* **66**, 366–372.
- Imarisio, S., Carmichael, J., Korolchuk, V., Chen, C.W., Saiki, S., Rose, C., Krishna, G., Davies, J.E., Ttofi, E., Underwood, B.R., et al. (2008). Huntington's disease: from pathology and genetics to potential therapies. *Biochem. J.* **412**, 191–209.
- Khoshnan, A., Ko, J., Watkin, E.E., Paige, L.A., Reinhart, P.H., and Patterson, P.H. (2004). Activation of the I $\kappa$ B kinase complex and nuclear factor- $\kappa$ B contributes to mutant huntingtin neurotoxicity. *J. Neurosci.* **24**, 7999–8008.
- Landouere, G., Zdebik, A.A., Martinez, T.L., Burnett, B.G., Stanescu, H.C., Inada, H., Shi, Y., Taye, A.A., Kong, L., Munns, C.H., et al. (2010). Mutations in TRPV4 cause Charcot-Marie-Tooth disease type 2C. *Nat. Genet.* **42**, 170–174.
- Leissring, M.A., Akbari, Y., Fanger, C.M., Cahalan, M.D., Mattson, M.P., and LaFerla, F.M. (2000). Capacitative calcium entry deficits and elevated luminal calcium content in mutant presenilin-1 knockin mice. *J. Cell Biol.* **149**, 793–798.
- Ma, H.T., Venkatachalam, K., Rys-Sikora, K.E., He, L.P., Zheng, F., and Gill, D.L. (2003). Modification of phospholipase C- $\gamma$ -induced Ca<sup>2+</sup> signal generation by 2-aminoethoxydiphenyl borate. *Biochem. J.* **376**, 667–676.
- Marsh, J.L., Lukacsovich, T., and Thompson, L.M. (2009). Animal models of polyglutamine diseases and therapeutic approaches. *J. Biol. Chem.* **284**, 7431–7435.
- Milnerwood, A.J., and Raymond, L.A. (2007). Corticostriatal synaptic function in mouse models of Huntington's disease: early effects of huntingtin repeat length and protein load. *J. Physiol.* **585**, 817–831.
- Montell, C. (2005). The TRP superfamily of cation channels. *Sci. STKE* **2005**, re3.
- Nakai, M., Qin, Z.H., Chen, J.F., Wang, Y., and Chase, T.N. (2000). Kainic acid-induced apoptosis in rat striatum is associated with nuclear factor- $\kappa$ B activation. *J. Neurochem.* **74**, 647–658.
- Narayanan, K.L., Irmady, K., Subramaniam, S., Unsicker, K., and von Bohlen and Halbach, O. (2008). Evidence that TRPC1 is involved in hippocampal glutamate-induced cell death. *Neurosci. Lett.* **446**, 117–122.
- Panov, A.V., Gutekunst, C.A., Leavitt, B.R., Hayden, M.R., Burke, J.R., Strittmatter, W.J., and Greenamyre, J.T. (2002). Early mitochondrial calcium defects in Huntington's disease are a direct effect of polyglutamines. *Nat. Neurosci.* **5**, 731–736.
- Petrucelli, L., and Dawson, T.M. (2004). Mechanism of neurodegenerative disease: role of the ubiquitin proteasome system. *Ann. Med.* **36**, 315–320.
- Putney, J.W., Jr. (2003). Capacitative calcium entry in the nervous system. *Cell Calcium* **34**, 339–344.
- Qin, Z.H., Wang, Y., Chen, R.W., Wang, X., Ren, M., Chuang, D.M., and Chase, T.N. (2001). Prostaglandin A(1) protects striatal neurons against excitotoxic injury in rat striatum. *J. Pharmacol. Exp. Ther.* **297**, 78–87.
- Qin, Z.H., Wang, Y., Nakai, M., and Chase, T.N. (1998). Nuclear factor- $\kappa$ B contributes to excitotoxin-induced apoptosis in rat striatum. *Mol. Pharmacol.* **53**, 33–42.
- Ravikumar, B., Vacher, C., Berger, Z., Davies, J.E., Luo, S., Oroz, L.G., Scaravilli, F., Easton, D.F., Duden, R., O'Kane, C.J., et al. (2004). Inhibition of mTOR induces autophagy and reduces toxicity of polyglutamine expansions in fly and mouse models of Huntington disease. *Nat. Genet.* **36**, 585–595.
- Riccio, A., Medhurst, A.D., Mattei, C., Kelsell, R.E., Calver, A.R., Randall, A.D., Benham, C.D., and Pangalos, M.N. (2002). mRNA distribution analysis of human TRPC family in CNS and peripheral tissues. *Brain Res. Mol. Brain Res.* **109**, 95–104.
- Roze, E., Saudou, F., and Caboche, J. (2008). Pathophysiology of Huntington's disease: from huntingtin functions to potential treatments. *Curr. Opin. Neurol.* **21**, 497–503.
- Selvaraj, S., Sun, Y., and Singh, B.B. (2010). TRPC channels and their implication in neurological diseases. *CNS Neurol. Disord. Drug Targets* **9**, 94–104.
- Selvaraj, S., Watt, J.A., and Singh, B.B. (2009). TRPC1 inhibits apoptotic cell degeneration induced by dopaminergic neurotoxin MPTP/MPP(+). *Cell Calcium* **46**, 209–218.
- Slaugenhaupt, S.A. (2002). The molecular basis of mucopolidiosis type IV. *Curr. Mol. Med.* **2**, 445–450.
- Slow, E.J., van Raamsdonk, J., Rogers, D., Coleman, S.H., Graham, R.K., Deng, Y., Oh, R., Bissada, N., Hossain, S.M., Yang, Y.Z., et al. (2003). Selective striatal neuronal loss in a YAC128 mouse model of Huntington disease. *Hum. Mol. Genet.* **12**, 1555–1567.
- Steffan, J.S., Bodai, L., Pallos, J., Poelman, M., McCampbell, A., Apostol, B.L., Kazantsev, A., Schmidt, E., Zhu, Y.Z., Greenwald, M., et al. (2001). Histone deacetylase inhibitors arrest polyglutamine-dependent neurodegeneration in *Drosophila*. *Nature* **413**, 739–743.
- Sugars, K.L., Brown, R., Cook, L.J., Swartz, J., and Rubinsztein, D.C. (2004). Decreased cAMP response element-mediated transcription: an early event in exon 1 and full-length cell models of Huntington's disease that contributes to polyglutamine pathogenesis. *J. Biol. Chem.* **279**, 4988–4999.
- Sun, Y., Savanenin, A., Reddy, P.H., and Liu, Y.F. (2001). Polyglutamine-expanded huntingtin promotes sensitization of N-methyl-D-aspartate receptors via post-synaptic density 95. *J. Biol. Chem.* **276**, 24713–24718.
- Supnet, C., Grant, J., Kong, H., Westaway, D., and Mayne, M. (2006). Amyloid-beta-(1–42) increases ryanodine receptor-3 expression and function in neurons of TgCRND8 mice. *J. Biol. Chem.* **281**, 38440–38447.
- Tang, T.S., Tu, H., Chan, E.Y., Maximov, A., Wang, Z., Wellington, C.L., Hayden, M.R., and Bezprozvanny, I. (2003). Huntingtin and huntingtin-associated protein 1 influence neuronal calcium signaling mediated by inositol-(1,4,5) triphosphate receptor type 1. *Neuron* **39**, 227–239.
- Tang, T.S., Slow, E., Lupu, V., Stavrovskaya, I.G., Sugimori, M., Liinas, R., Kristal, B.S., Hayden, M.R., and Bezprozvanny, I. (2005). Disturbed Ca<sup>2+</sup> signaling and apoptosis of medium spiny neurons in Huntington's disease. *Proc. Natl. Acad. Sci. USA* **102**, 2602–2607.
- Tang, T.S., Guo, C., Wang, H., Chen, X., and Bezprozvanny, I. (2009). Neuroprotective effects of inositol 1,4,5-trisphosphate receptor C-terminal fragment in a Huntington's disease mouse model. *J. Neurosci.* **29**, 1257–1266.
- Thompson, L.M., Aiken, C.T., Kaltenbach, L.S., Agrawal, N., Illes, K., Khoshnan, A., Martinez-Vincente, M., Arrasate, M., O'Rourke, J.G., Khashwji, H., et al. (2009). IKK phosphorylates Huntingtin and targets it for degradation by the proteasome and lysosome. *J. Cell Biol.* **187**, 1083–1099.



- Tobe, M., Isobe, Y., Tomizawa, H., Nagasaki, T., Takahashi, H., Fukazawa, T., and Hayashi, H. (2003a). Discovery of quinazolines as a novel structural class of potent inhibitors of NF-kappa B activation. *Bioorg. Med. Chem.* *11*, 383–391.
- Tobe, M., Isobe, Y., Tomizawa, H., Nagasaki, T., Takahashi, H., and Hayashi, H. (2003b). A novel structural class of potent inhibitors of NF-kappa B activation: structure-activity relationships and biological effects of 6-aminoquinazoline derivatives. *Bioorg. Med. Chem.* *11*, 3869–3878.
- Venkatachalam, K., Long, A.A., Elsaesser, R., Nikolaeva, D., Broadie, K., and Montell, C. (2008). Motor deficit in a *Drosophila* model of mucopolipidosis type IV due to defective clearance of apoptotic cells. *Cell* *135*, 838–851.
- Venkiteswaran, G., and Hasan, G. (2009). Intracellular Ca<sup>2+</sup> signaling and store-operated Ca<sup>2+</sup> entry are required in *Drosophila* neurons for flight. *Proc. Natl. Acad. Sci. USA* *106*, 10326–10331.
- Vonsattel, J.P., and DiFiglia, M. (1998). Huntington disease. *J. Neuropathol. Exp. Neurol.* *57*, 369–384.
- Wenning, A.S., Neblung, K., Strauss, B., Wolfs, M.J., Sappok, A., Hoth, M., and Schwarz, E.C. (2011). TRP expression pattern and the functional importance of TRPC3 in primary human T-cells. *Biochim. Biophys. Acta* *1813*, 412–423.
- Wu, J., Tang, T., and Bezprozvanny, I. (2006). Evaluation of clinically relevant glutamate pathway inhibitors in in vitro model of Huntington's disease. *Neurosci. Lett.* *407*, 219–223.
- Wu, J., Li, Q., and Bezprozvanny, I. (2008). Evaluation of Dimebon in cellular model of Huntington's disease. *Mol. Neurodegener.* *3*, 15.
- Wu, J., Jeong, H.K., Bulin, S.E., Kwon, S.W., Park, J.H., and Bezprozvanny, I. (2009). Ginsenosides protect striatal neurons in a cellular model of Huntington's disease. *J. Neurosci. Res.* *87*, 1904–1912.
- Yamamoto, S., Wajima, T., Hara, Y., Nishida, M., and Mori, Y. (2007). Transient receptor potential channels in Alzheimer's disease. *Biochim. Biophys. Acta* *1772*, 958–967.
- Yang, K.T., Chen, W.P., Chang, W.L., Su, M.J., and Tsai, K.L. (2005). Arachidonic acid inhibits capacitative Ca<sup>2+</sup> entry and activates non-capacitative Ca<sup>2+</sup> entry in cultured astrocytes. *Biochem. Biophys. Res. Commun.* *331*, 603–613.
- Yoo, A.S., Cheng, I., Chung, S., Grenfell, T.Z., Lee, H., Pack-Chung, E., Handler, M., Shen, J., Xia, W., Tesco, G., et al. (2000). Presenilin-mediated modulation of capacitative calcium entry. *Neuron* *27*, 561–572.
- Zeron, M.M., Hansson, O., Chen, N., Wellington, C.L., Leavitt, B.R., Brundin, P., Hayden, M.R., and Raymond, L.A. (2002). Increased sensitivity to N-methyl-D-aspartate receptor-mediated excitotoxicity in a mouse model of Huntington's disease. *Neuron* *33*, 849–860.
- Zhang, Y., Leavitt, B.R., van Raamsdonk, J.M., Dragatsis, I., Goldowitz, D., MacDonald, M.E., Hayden, M.R., and Friedlander, R.M. (2006). Huntingtin inhibits caspase-3 activation. *EMBO J.* *25*, 5896–5906.
- Zhang, H., Li, Q., Graham, R.K., Slow, E., Hayden, M.R., and Bezprozvanny, I. (2008). Full length mutant huntingtin is required for altered Ca<sup>2+</sup> signaling and apoptosis of striatal neurons in the YAC mouse model of Huntington's disease. *Neurobiol. Dis.* *31*, 80–88.